2012

# Face Recognition with Degraded Images

Iman Makaremi
*University of Windsor*

# Face Recognition with Degraded Images

by

**Iman Makaremi**

A Dissertation
Submitted to the Faculty of Graduate Studies through the
Department of Electrical and Computer Engineering in Partial Fulfilment
of the Requirements for the Degree of Doctor of Philosophy at the
University of Windsor

Windsor, Ontario, Canada
2012

Library and Archives Canada

Published Heritage Branch

395 Wellington Street
Ottawa ON K1A 0N4
Canada

Bibliothèque et Archives Canada

Direction du Patrimoine de l'édition

395, rue Wellington
Ottawa ON K1A 0N4
Canada

Your file Votre référence
ISBN: 978-0-494-78280-4

Our file Notre référence
ISBN: 978-0-494-78280-4

Face Recognition with Degraded Images

by

Iman Makaremi

APPROVED BY:

---

M. Orchard, External Examiner
Electrical and Computer Engineering, Rice University

---

B. Boufama
Computer Science, University of Windsor

---

M. A. S. Khalid
Electrical and Computer Engineering, University of Windsor

---

J. Wu
Electrical and Computer Engineering, University of Windsor

---

M. Ahmadi, Advisor
Electrical and Computer Engineering, University of Windsor

January 5, 2012

# *Declaration of Previous Publication*

This thesis includes 4 original papers that have been previously published/submitted for publication in peer reviewed journals and conferences, as follows:

| Thesis Chapter | Publication Title | Publication Status |
|---|---|---|
| Chapter 2 | Blur Invariants: A Novel Representation in the Wavelet Domain | Published |
| Chapter 2 | Wavelet Domain Blur Invariants for 1D Discrete Signals | Published |
| Chapter 2 | Wavelet Domain Blur Invariants for Image Analysis | Published |
| Chapter 3 | Face Recognition with Blurred Images using an Alternative Definition for Moment based Blur Invariant Descriptors | Submitted |

I certify that I have obtained a written permission from the copyright owner(s) to include the above published material(s) in my thesis. I certify that the above material describes work completed during my registration as graduate student at the University of Windsor.

I certify that, to the best of my knowledge, my thesis does not infringe upon anyones copyright nor violate any proprietary rights and that any ideas, techniques, quotations, or any other material from the work of other people included in my thesis, published or otherwise, are fully acknowledged in accordance with the standard referencing practices. Furthermore, to the extent that I have included copyrighted material that surpasses the bounds of fair dealing within the meaning of the Canada Copyright Act, I certify that I have obtained a written permission from the copyright owner(s) to include such material(s) in my thesis and have included copies of such copyright clearances to my appendix.

I declare that this is a true copy of my thesis, including any final revisions, as approved by my thesis committee and the Graduate Studies office, and that this thesis has not been submitted for a higher degree to any other University or Institution.

# *Abstract*

After more than two decades of research on the topic, automatic face recognition is finding its applications in our daily life; banks, governments, airports and many other institutions and organizations are showing interest in employing such systems for security purposes. However, there are so many unanswered questions remaining and challenges not yet been tackled. Despite its common occurrence in images, blur is one of the topics that has not been studied until recently.

There are generally two types of approached for dealing with blur in images: 1) identifying the blur system in order to restore the image, 2) extracting features that are blur invariant. The first category requires extra computation that makes it expensive for large scale pattern recognition applications. The second category, however, does not suffer from this drawback. This class of features were proposed for the first time in 1995, and has attracted more attention in the last few years. The proposed invariants are mostly developed in the spatial domain and the Fourier domain. The spatial domain blur invariants are developed based on moments, while those in the Fourier domain are defined based on the phase' properties.

In this dissertation, wavelet domain blur invariants are proposed for the first time, and their performance is evaluated in different experiments. It is also shown that the spatial domain blur invariants are a special case of the proposed invariants.

The second contribution of this dissertation is blur invariant descriptors that are developed based on an alternative definition for ordinary moments that is proposed in this dissertation for the first time. These descriptors are used for face recognition with blurred images, where excellent results are achieved. Also, in a comparison with the state-of-art, the superiority of the proposed technique is demonstrated.

To the most valuable part of my life, my family, for their unending love and support.

# *Acknowledgments*

There are several people who deserve my sincere thanks for their generous contributions to this project. I would first like to express my sincere gratitude and appreciation to Dr. Majid Ahmadi, my supervisor for his invaluable guidance and constant support throughout the course of this work. I would also like to thank my committee members Dr. Boubakeur Boufama, Dr. Mohammed Khalid, and Dr. Jonathan Wu and Dr. Michael Orchard for their participation in my seminars, reviewing my dissertation, and their constructive comments.

Finally, my deepest gratitude goes to my family for their unconditional love, support and encouragement.

# Contents

# List of Figures

# List of Tables

# *List of Abbreviations*

| | |
|---|---|
| 1D | One Dimensional |
| 2D | Two Dimensional |
| BID | Blur Invariant Descriptor |
| CWT | Continuous Wavelet Transform |
| DSP | Digital Signal Processing |
| DWT | Discrete Wavelet Transform |
| EEG | Electroencephalography |
| EM | Eigen Moment |
| GOM | Generalized Ordinary Moment |
| JPEG | Joint Photographic Experts Group |
| LH | Local Histogram |
| LPQ | Local Phase Quantisation |
| NN | Nearest Neighbour |
| PCA | Principal Component Analysis |
| PSF | Point Spread Function |
| SDBI | Spatial Domain Blur Invariant |
| WDBI | Wavelet Domain Blur Invariant |

# Chapter 1

# *Introduction and Preliminary Concepts and Definitions*

## 1.1 Introduction

The face is known to be a very important communication channel in our daily lives, through which we express our feelings and understand others', recognize people, and so on. Such abilities are so integrated in our brain that we do not even realize what a complicated task is being done.

The face is indeed the most favourable biometric feature that everyone carries around with no will of losing it, making it an easy and non-invasive medium for identification, recognition, human-computer interaction, to call a few. Such unique properties have caused a growing demand in automatic face recognition systems by governments, banks, law enforcement, airports, etc., and the accessibility of powerful computers and fast networks made the realization of such systems only a pattern recognition problem.

In its simplest setup, the face recognition problem tries to identify an individual from a set of images of different people. The images are mostly taken in controlled environments, in order to avoid pose and illumination variations. The currently available face recognition systems report relatively higher recognition rate in comparison with human on such databases.

However, our natural embedded face recognition system proves to be more robust as soon as the imaging condition is not ideal [9, 38, 27]. Changes in pose and illumination and those caused by blur,

face expression, occlusion, make-up, and natural processes such as ageing and weight changes are a few challenges that are encountered by practical face recognition systems. Some of these challenges have received attention of researchers in the field. For example, pose and illumination variations are two topics that have been studied comprehensively, and there is even a designated database for them [22].

On the other hand, other topics have not been addressed. Ageing, for example, is a challenge that face recognition systems need to deal with as they must accommodate such changes by their subjects. However, the lack of a suitable database to this date has hindered a real-world study on this issue, forcing the researchers to synthetically model it [40]. Another recently raised concern is the vulnerability of automatic face recognition systems to cosmetic surgery [29]. The logic behind this issue is as the same as the one for ageing, plus the fact that the probability of being caught in such a situation is low. However, if a bank wants to use such systems to identify their costumers, they are required to respect their decision, and that leads to a challenge that should be accepted by the researchers.

Contrastingly with the issues that might be considered as the worries of tomorrow, blur, which is one of the inevitable challenges in unconstrained face recognition problems[9], has been overlooked until recently. Movement of the subject, an unfocused camera, or a long distance between the subject and the camera introduce blur to the acquired image, which can drastically affect the performance of a face recognition system. Having robust to blur or blur invariant techniques that can tackle such problems sounds necessary. Most of the techniques that have been proposed so far are based on deblurring the query image prior to recognition, which requires a preprocessing step and translates into extra computation. With an increasing volume of videos from surveillance cameras and the need of going through a lot of them to find a suspect in some instances, a deblurring step before recognition is definitely not a reasonable idea. Thus, using features that are robust - or even better, invariant - to blur is an alternative approach that can eliminate the need for such tedious preprocesses.

The first category of blur invariants [18] was introduced for the first time with a similar intention: to avoid deblurring which is an ill-posed problem. The proposed blur invariants were developed based on geometric moments and in the spatial domain. It was not almost until ten years later when other researchers showed interest in developing such features as well, but unfortunately most of their efforts were shown to be redundant [30]. Along with the moment based blur invariants, another set of such invariants were developed in the Fourier domain [18]. Unlike the first set, the proposed modifications and extensions on this set of invariants are promising.

Unlike the Fourier domain blur invariants, the moment based blur invariants have not been employed

in challenging pattern recognition problems. Most of the applications that have been reported for these invariants are image registration and remote sensing [20]. This became a motivation to use these invariants for face recognition to explore their performance in such problems. Also, the available blur invariants are developed either in the spatial domain or Fourier domain, which raises this question: is it possible to develop blur invariants in the wavelet domain in order to take advantage of the extra properties that this domain has? In the next chapter, moment based blur invariants in the wavelet domain are proposed for the first time as an answer to this question. In chapter 3, the moment based blur invariants are employed for face recognition. Also an alternative way of dealing with moments is proposed in that chapter in order to increase their discriminablity, which yields promising results.

The preliminary definitions and concepts that are required in this dissertation are given in the next two sections. Section 1.2 is dedicated to wavelet transform. In this section, the general concepts of wavelet transform are reviewed, and three different types of wavelet transforms for 1D and 2D signals are presented. Section 1.3 provided a review of geometric moments for 1D and 2D signals.

## 1.2 Wavelet Transform

Wavelet transform [12] has been used widely in many fields such as JPEG2000 [70]. A growing number of publications deal with hardware implementation of this transform [60, 33, 49, 66] which demonstrate its utility in the area of DSP and Pattern Recognition. A multi-resolution analysis of signals with localization in both time and frequency is the advantage of wavelet transform over Fourier and cosine transforms [12, 48]. Also, having different alternatives for the basis function in wavelet transform makes it more adaptable for different problems than Fourier transform since in the latter only one kind of basis function can be used.

In the rest of this section, continuous and discrete wavelet transforms are reviewed. Also, a specific type of discrete wavelet transform is introduced, which is shift invariant.

### 1.2.1 Continuous Wavelet Transform

The continuous wavelet transform (CWT) of a 1D continuous signal $f(x)$ at shift $u$ and scale $s$ with wavelet function $\psi(x)$ is [46]

$$\hat{f}^{\psi}(s,u) = \int_{-\infty}^{+\infty} \frac{1}{\sqrt{s}} f(x) \psi^* \left( \frac{x-u}{s} \right) dx. \tag{1.1}$$

where $\psi^*(\cdot)$ is the complex conjugate of $\psi(\cdot)$.

### 1.2.2 Discrete Wavelet Transform

The wavelet coefficients of 1D discrete signal $x$ are calculated with a cascade of discrete convolutions and sub-sampling.

$$a_{j+1}[n] = \left(\bar{h} \star a_j[n]\right) \downarrow 2, \tag{1.2}$$

$$d_{j+1}[n] = \left(\bar{g} \star a_j[n]\right) \downarrow 2, \tag{1.3}$$

where $a_0 = x$, $j = 0, \cdots, J-1$, $h$ and $g$ are scaling and wavelet filters, respectively, $\bar{h}[n] = h^*[-n]$, and $\bar{g}[n] = g^*[-n]$. $a_{j+1}$ is the approximation coefficient and $d_{j+1}$ is the detail coefficient at level $j+1$.

If $x$ is a 2D discrete signals, the wavelet coefficients are calculated as follows:

$$a_{j+1}[n_1, n_2] = \left(\bar{h}\bar{h} \star a_j[n_1, n_2]\right) \downarrow 2, \tag{1.4}$$

$$d^1_{j+1}[n_1, n_2] = \left(\bar{h}\bar{g} \star a_j[n_1, n_2]\right) \downarrow 2, \tag{1.5}$$

$$d^2_{j+1}[n_1, n_2] = \left(\bar{g}\bar{h} \star a_j[n_1, n_2]\right) \downarrow 2, \tag{1.6}$$

$$d^3_{j+1}[n_1, n_2] = \left(\bar{g}\bar{g} \star a_j[n_1, n_2]\right) \downarrow 2. \tag{1.7}$$

where $a_0 = x$, $j = 0, \cdots, J-1$, $a_{j+1}$ is the approximation coefficient, and $d^i_{j+1}$ is the $i^{\text{th}}$ detail coefficient at level $j+1$. The block diagram of the discrete wavelet decomposition is illustrated in Figure 1.1.

### 1.2.3 Shift Invariant Discrete Wavelet Transform

DWT suffers from a major drawback: it is not shift invariant (also called translation invariant in the literature), and this is due to the dyadic sub-sampling [47, 31]. In order to make the moments

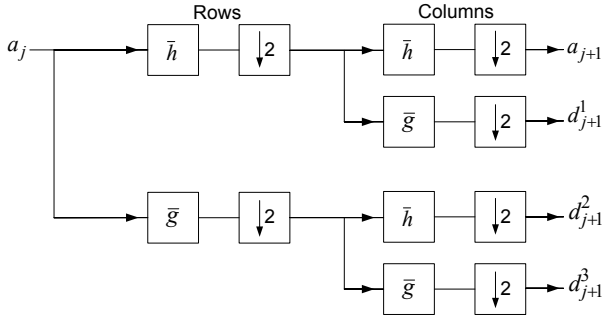


Figure 1.1: Decomposition in Discrete Wavelet Transform

invariant to shift, it is necessary to have a shift invariant wavelet transform. There have been several different techniques developed to produce shift invariant wavelet transforms. Continuous Wavelet Transform (CWT) does not suffer from the same drawback as its counterpart in the discrete domain [46]. Therefore, it is typically utilized when the wavelet transform is only required at a few specific scales. Mallat proposed a scheme [45] that is an approximation of CWT, which was later proved to be shift invariant[67]. *À trous* algorithm [46] is the simplest and yet an effective technique that is proposed to make DWT invariant to shift. In this technique, the sub-sampling operator is removed, and the filters are instead up-sampled at each level by inserting zeros between every two coefficients [46]. Over Complete DWT (OCDWT) [6] is another proposed technique which guarantees an approximately shift invariant implementation of wavelet transform if the level below is fully sampled. Shift invariance has been also achieved by calculating the wavelet transform of all shifts [34].

In this dissertation, the *à trous* algorithm is used. In this algorithm, scaling and wavelet filters at scale $j+1$ are defined as

$$h_{j+1}[k] = h_j[k]\uparrow 2 = \begin{cases} h_j[\frac{k}{2}], & k \text{ even} \\ 0, & k \text{ odd} \end{cases} \tag{1.8}$$

$$g_{j+1}[k] = g_j[k]\uparrow 2 = \begin{cases} g_j[\frac{k}{2}], & k \text{ even} \\ 0, & k \text{ odd} \end{cases} \tag{1.9}$$

where $h_0[k] = h[k]$ and $g_0[k] = g[k]$. The wavelet coefficients of 1D discrete signal $x$ are calculated with a cascade of discrete convolutions.

$$a_{j+1}[n] = \bar{h}_j \star a_j[n], \tag{1.10}$$

$$d_{j+1}[n] = \bar{g}_j \star a_j[n], \tag{1.11}$$

where $a_0 = x$, $j = 0, \cdots, J-1$. In this dissertation, the wavelet coefficients (either approximation or detail) of signal $x$ at level $f_0 f_1 \cdots f_{L-1}$ are called $\overset{\psi_L}{W}x$, which is related to $x$ as

$$\overset{\psi_L}{W}x[n] = \bar{\psi}_L \star x[n], \tag{1.12}$$

where

$$\psi_L[n] = f_0 \star \cdots \star f_{L-1}[n], \tag{1.13}$$

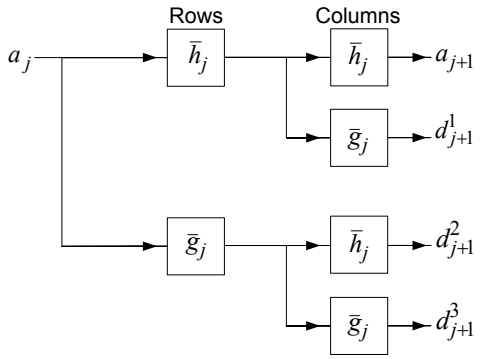


Figure 1.2: Decomposition in Redundant Wavelet Transform

and $f$ is either $h$ or $g$.

Similarly, if $x$ is a 2D discrete signal, its wavelet coefficients are calculated as follows:

$$a_{j+1}[n_1, n_2] = \bar{h}_j \bar{h}_j \star a_j[n_1, n_2], \tag{1.14}$$

$$d^1_{j+1}[n_1, n_2] = \bar{h}_j \bar{g}_j \star a_j[n_1, n_2], \tag{1.15}$$

$$d^2_{j+1}[n_1, n_2] = \bar{g}_j \bar{h}_j \star a_j[n_1, n_2], \tag{1.16}$$

$$d^3_{j+1}[n_1, n_2] = \bar{g}_j \bar{g}_j \star a_j[n_1, n_2]. \tag{1.17}$$

where $a_0 = x$, and $j = 0, \cdots, J-1$. The block diagram of this transform is presented in Figure 1.2.

The wavelet coefficients (either approximation or detail) of signal $x$ at level $f^1_0 f^1_1 \cdots f^1_{L-1} – f^2_0 f^2_1 \cdots f^2_{L-1}$ are called $\overset{\psi_L}{W} x$, which is related to $x$ as

$$\overset{\psi_L}{W} x[n_1, n_2] = \bar{\psi}_L \star x[n_1, n_2], \tag{1.18}$$

where

$$\psi_L[n_1, n_2] = \psi^1_L[n_1] \psi^2_L[n_2], \tag{1.19}$$

$$\psi^1_L[n_1] = f^1_0 \star \cdots \star f^1_{L-1}[n_1], \tag{1.20}$$

$$\psi^2_L[n_2] = f^2_0 \star \cdots \star f^2_{L-1}[n_2], \tag{1.21}$$

and $f$ is either $h$ or $g$.

### 1.2.4 Vanishing Moment

The wavelet function $\psi \in L^2(\mathbb{Z})$ has $M_\psi$ vanishing moments (also called zero moments) if

$$\int_{-\infty}^{+\infty} t^p \psi(t)\, dt = 0, \qquad \text{for } p \leq M_\psi. \tag{1.22}$$

The number of vanishing moments of $\psi$ is equal to the number of zeros of its Fourier transform,$\hat{\psi}(w)$, at $w = 0$ [46]. $M_\psi$ depends on the number of zeros of $g$'s Fourier transform, $\hat{g}(w)$, at $w = 0$, $M_g$, and its repetition in obtaining $\psi$, $N$. Since the scaling filter designed such that $\hat{h}(0) = \sqrt{2}$, we can easily show that $M_\psi = NM_g$. Therefore, if $\psi_L \in \mathbf{L}^2\left(\mathbb{Z}^2\right)$, and it consists of $N_i$ wavelet filters on the $i^{\text{th}}$ dimension $(i = 1, 2)$, then it has $M_{\psi_L^i} = N_i M_g$ on that dimension.

## 1.3 Moments

In this section, some of the basic terms for moments are defined and explained.

### 1.3.1 Moments for Continuous Signals

The $p^{\text{th}}$ order ordinary geometric moment of 1D continuous signal $f(x)$ in the spatial domain is defined by [59]

$$m_p^f = \int_{-\infty}^{+\infty} x^p f(x) dx. \tag{1.23}$$

The centroid of signal $f(x)$ is [59]

$$c^f = \frac{m_1^f}{m_0^f}. \tag{1.24}$$

The $p^{\text{th}}$ order central moment of 1D continuous signal $f(x)$ in the spatial domain is defined by [59]

$$\mu_p^f = \int_{-\infty}^{+\infty} \left(x - c^f\right)^p f(x) dx. \tag{1.25}$$

### 1.3.2 Moments for Discrete Signals

The $p^{\text{th}}$ order ordinary geometric moment of 1D discrete signal $x$ in the spatial domain is defined by

$$m_p^x = \sum_n n^p x[n]. \tag{1.26}$$

The centroid of signal $x$ is

$$c^x = \frac{m_1^x}{m_0^x} \tag{1.27}$$

The $p^{\text{th}}$ order central moment of 1D discrete signal $x$ in the spatial domain is defined by

$$\mu_p^x = \sum_n (n - c^x)^p \, x[n]. \tag{1.28}$$

If the discrete signal $x$ is 2D, its ordinary geometric moment of order $(p+q)$ in the spatial domain is defined by

$$m_{p,q}^x = \sum_{n_1} \sum_{n_2} n_1^p n_2^q x[n_1, n_2]. \tag{1.29}$$

The centroid of signal $x$ is

$$c_1^x = \frac{m_{1,0}^x}{m_{0,0}^x}, \; c_2^x = \frac{m_{0,1}^x}{m_{0,0}^x}. \tag{1.30}$$

The central moment of order $(p+q)$ of 2D discrete signal $x$ in the spatial domain is defined by

$$\mu_{p,q}^x = \sum_{n_1} \sum_{n_2} (n_1 - c_1)^p \, (n_2 - c_2)^q \, x[n_1, n_2]. \tag{1.31}$$

It is worth mentioning that there are some other definitions available for moments which happen to be orthogonal as well. However, only geometric moments are exploited in this dissertation for proposing new algorithms. This does not deny the possibility of developing them based on orthogonal moments. This matter is discussed further in Chapter 3.

# Chapter 2

# *Blur Invariants: A Novel Representation in the Wavelet Domain*

## 2.1 Introduction

Signal acquisition is the first step in all signal processing tasks, and is always accompanied with different sources of degradation. The effect of some of the degradations is considerably high, which could vastly affect expected outcomes. People in surveillance photos and body parts in medical images are real-world subjects that are not ideally controllable when acquiring images. Environmental situations might also have a negative effect on the quality of signals, e.g. weather condition and long distances between camera and subject can deteriorate images. Deteriorations in images are basically of two types: geometric distortions, and radiometric degradations. The first type includes the distortions such as translation, scaling, and rotation. There are many different approaches in literature which are proposed for dealing with these problems. Hu, for the first time, proposed descriptors that are invariant to some of the basic linear geometric distortions [26]. Recently a novel approach has been put forward by Flusser et al. [15], where implicit moment invariants are introduced for dealing with nonlinear deformations. For surveys on similar invariants refer to [64, 74, 20].

Unlike geometric distortions, there are fewer research works carried out on radiometric degradations. They are generally introduced to images due to the movement of subject, unfocused camera, and non-ideal image capturing environment. The general model that is commonly used for the observed

signal is

$$g(\mathbf{x}) = Hf(\mathbf{x}) + n(\mathbf{x}) \tag{2.1}$$

In this model, $g$ is the observed signal, $f$ and $n$ are the actual signal and noise, respectively, and $H$ is the degradation operator. It is assumed that $H$ is linear and space-invariant, and the general model can be simplified to

$$g(\mathbf{x}) = f(\mathbf{x}) \star h(\mathbf{x}) + n(\mathbf{x}), \tag{2.2}$$

where '$\star$' denotes the convolution, and $h$ is the Point Spread Function (PSF) of the system.

The proposed approaches for dealing with blur can be categorized into two types: 1) blind restoration, and 2) direct analysis. In blind restoration techniques, the purpose is to identify the blur system model and extract the actual signal [65, 32]. The main application of these methods is in signal restoration. There are also similar techniques in which the effort is to only restore the features of degraded signals [23], with their main application in pattern recognition. Although these techniques have been vastly used, they suffer from major drawbacks: deblurring is an ill-posed problem, and because of the identification part, they are computationally expensive, while it is not required to identify the blur system in many applications.

The second type of techniques focus on developing descriptors that are inherently invariant to blur. The main advantage of these methods is that they do not go through the process of identifying the blur system. Flusser et al. [18] established this type for the first time. Their invariant descriptors were developed in the spatial domain and based on geometric moments. Their assumption was that the blur operator is symmetric. Later, they represented a closed format of the invariants [19], and added extra properties to the descriptors in order to make them invariant to geometric distortions while changing their assumption for the blur systems to centrally symmetric[17, 69]. They also developed these invariants for 1D signals [16]. Utilizing complex moments, Flusser and Zitovà [21] proposed descriptors that are both invariant to centrally symmetric blur and rotation. Liu and Zhang [39] also developed similar blur invariants using complex moments. Metari and Deschênes [50] exploited the Mellin transform properties in order to define a different representation of geometric-moment-based blur invariant descriptors. They also showed that their proposed descriptors are invariant to a few geometric distortions as well. Instead of using geometric moments, Zhang et al. [76] employed Legendre moments in order to define their invariants in the spatial domain. On the other hand, Ji and Zhu [28] proved that the Zernike moments ,$Z_{pq}$, are inherently invariant to Gaussian blur when $p = q$.

Along with the blur invariant descriptors defined in the spatial domain, there are some other methods that are developed in the Fourier domain. Flusser and Suk [16] proposed their Fourier based

invariants for 1D signals based on the tangent of the phase of signals, and proved that they are invariant to blur. They developed this representation for 2D signals and showed their relationship with their invariants in the spatial domain [17]. These invariants were later developed for $n$D signals and made to be invariant to some of the geometric distortions [14]. Ojansivu and Heikkilä [57], however, showed that Flusser's invariants are sensitive to noise when implemented in the Fourier domain because of their use of tangent operator. They proposed a different representation of invariants in the Fourier domain. Subsequently, they made them invariant to the affine transform as well [56].
Blur moment invariants showed their practicality in a vast area of research: image registration [17, 55], remote sensing [5, 4], forgery detection [41], recognition [19, 39, 10], stereo matching [61], and control point extraction [3].
In this chapter, wavelet domain descriptors are proposed which are invariant to centrally symmetric blur systems. The immediate advantages of these invariants come from the domain that they are developed in: the different alternatives that exist for wavelet functions and the benefit of analysing signals at different scales in the wavelet domain. The wavelet domain blur invariants are first developed for 1D continuous signals. With a slight modification they are also presented for 1D and 2D discrete signals. This chapter is organized as follows. In section 2.2, the representation of blur in the wavelet domain for 1D continuous signals is shown first. Then, the relationship between the moments of the blurred signal in the wavelet domain and those of the original signal in the same domain are extracted. Using this relation, the blur invariants for 1D continuous signals are proposed and proved. The performance of these invariants is evaluated in section 2.3 against noise and blur changes and compared with the performance of the spatial domain blur invariants. Section 2.4 is devoted to extracting blur invariants for 1D discrete signals. In section 2.5, the performance of the developed invariants is evaluated in an experiment with two electroencephalography (EEG) signals. The wavelet domain blur invariants for 2D discrete signals are proposed in section 2.6, and analysed comprehensively in section 2.7 in three different experiments. There might be some special cases where the spatial domain and wavelet domain blur invariants cannot discriminate different signals. This discussion comes in section 2.8. The chapter is concluded in section 2.9.

## 2.2 Blur Invariants for 1D Continuous Signals

For 1D continuous signals, the wavelet transform is calculated with CWT (eq. 1.1), and the moments are obtained using (1.23) - (1.25).

### 2.2.1 Blur in the Wavelet Domain for 1D Continuous Signals

First, it will be shown that how (2.2) would be presented in the wavelet domain. Also for the sake of simplicity, noise is not shown in the equations. However, its effect on the invariants will be shown in section 2.3. The wavelet transform of blurred continuous signal $g(x)$ at shift $u$ and scale $s$ with wavelet function $\psi(x)$ is

$$\hat{g}^{\psi}(s,u) = \int_{-\infty}^{+\infty} \frac{1}{\sqrt{s}} g(x) \psi^{*}\left(\frac{x-u}{s}\right) dx. \tag{2.3}$$

Replacing $g(x)$ by its equivalent in (2.2) gives

$$\hat{g}^{\psi}(s,u) = \int_{-\infty}^{+\infty} \int_{-\infty}^{+\infty} \frac{1}{\sqrt{s}} h(y) f(x-y) \psi^{*}\left(\frac{x-u}{s}\right) dy dx. \tag{2.4}$$

Substituting $z$ for $x-y$, the above equation changes to

$$\begin{aligned} \hat{g}^{\psi}(s,u) &= \int_{-\infty}^{+\infty} h(y) \int_{-\infty}^{+\infty} \frac{1}{\sqrt{s}} f(z) \psi^{*}\left(\frac{z-(u-y)}{s}\right) dz dy \\ &= \int_{-\infty}^{+\infty} h(y) \hat{f}^{\psi}(s,u-y) dy \end{aligned} \tag{2.5}$$

which shows that the wavelet transform of $g(x)$ is the convolution of $h(x)$ by the wavelet transform of $f(x)$:

$$\hat{g}^{\psi}(s,u) = \hat{f}^{\psi}(s,u) \star h(u). \tag{2.6}$$

### 2.2.2 Moments in the Wavelet Domains for 1D Continuous Signals

Before expressing the relation between the moments of $\hat{g}^{\psi}(u,s)$ and those of $\hat{f}^{\psi}(u,s)$ and $h(u)$, it is shown how the moments of $f(x)$ in the wavelet domain are related to those in the spatial domain. Rewriting moments of continuous signals (eq. 1.3) for $\hat{f}^{\psi}(u,s)$, the wavelet transform of $f(x)$ with wavelet function $\psi(\cdot)$ at shift $u$ and scale $s$, we have the following:

$$\begin{aligned} m_p^{\hat{f}^{\psi}}(s) &= \int_{-\infty}^{+\infty} u^p \hat{f}^{\psi}(s,u) du \\ &= \frac{1}{\sqrt{s}} \int_{-\infty}^{+\infty} \int_{-\infty}^{+\infty} u^p f(x) \psi^{*}\left(\frac{x-u}{s}\right) dx du \\ &= \sqrt{s} \int_{-\infty}^{+\infty} \int_{-\infty}^{+\infty} (x-sy)^p f(x) \psi^{*}(y) dx dy. \end{aligned} \tag{2.7}$$

In (2.7), $y$ is substituted for $\left(\frac{x-u}{s}\right)$. Considering the fact that $(a+b)^p = \sum_{k=0}^{p} \binom{p}{k} a^k b^{p-k}$, the relation between the ordinary moments of signal $f(x)$ in the wavelet domain and the spatial domain can be extracted:

$$m_p^{\hat{f}^{\psi}}(s) = \sum_{k=0}^{p} \binom{p}{k} s^{k+\frac{1}{2}} (-1)^k m_{p-k}^{f} m_k^{\psi}. \tag{2.8}$$

It can be concluded from (2.8) that the moments of the wavelet transform of a signal with a wavelet function which has $M_\psi$ vanishing moments are zero up to order $M_\psi - 1$. Therefore, it would be impossible to calculate the centroid (eq. 1.24) for such signals since the denominator can become zeros. This also makes it impossible to take advantage of central moments. In order to be able to take advantage of central moments for such signals, a generalized definition of centroid is proposed, which appeared in [42] for the first time.

**Definition 1.** *If the moments of signal $f(x)$ are zero up to order $M-1$, its centroid is defined as*

$$\varsigma^f = \frac{m^f_{M+1}}{(M+1)m^f_M}. \tag{2.9}$$

It is trivial to show that $c^f$ is a special case of $\varsigma^f$, where $M = 0$.
The relation between the $p^{th}$ order central moment of $\hat{g}^\psi(s,u)$ and the central moments of $\hat{f}^\psi(s,u)$ and $h(x)$ can be extracted by rewriting (1.25) for $\hat{g}^\psi(s,u)$ with the generalized centroid definition (2.9), using (2.6), and considering the fact that $\varsigma^{\hat{g}^\psi} = \varsigma^{\hat{f}^\psi} + c^h$.

$$\begin{aligned}
\mu^{\hat{g}^\psi}_p(s) &= \int_{-\infty}^{+\infty} \left(u - \varsigma^{\hat{g}^\psi}\right)^p \hat{g}^\psi(s,u)du \\
&= \int_{-\infty}^{+\infty}\int_{-\infty}^{+\infty} \left(u - \varsigma^{\hat{g}^\psi}\right)^p \hat{f}^\psi(s,u)h(v-u)dvdu \\
&= \sum_{k=0}^{p} \binom{p}{k} \mu^{\hat{f}^\psi}_k(s)\, \mu^h_{p-k}.
\end{aligned} \tag{2.10}$$

If the employed wavelet function has $M_\psi$ vanishing moments, by defining $q + M_\psi = p$, $\acute{\mu}_q(s) = \mu_p(s)$, and $\binom{q}{l}_{M_\psi} = \binom{q+M\psi}{l+M\psi}$, the above equation can be simplified into:

$$\acute{\mu}^{\hat{g}^\psi}_q(s) = \sum_{l=0}^{q} \binom{q}{l}_{M_\psi} \acute{\mu}^{\hat{f}^\psi}_l(s)\, \mu^h_{q-l}. \tag{2.11}$$

It shows that the central moments of $\hat{g}^\psi(s,u)$ of a certain order are related to the central moments of $\hat{f}^\psi(s,u)$ and $h(x)$ of the same and lower orders.

### 2.2.3 Wavelet Domain Blur Invariants for 1D Continuous Signals

In order to extract blur invariant features, it is necessary to look for combinations of moments such that those of $h(x)$ would be eliminated. It is assumed that $h(x)$, the PSF, is symmetric and energy-preserving. When $h(x)$ is symmetric, i.e. $h(x) = h(-x)$, its odd order moments are zero. And because of the energy-preserving property, the integral $\int_{-\infty}^{+\infty} h(x)dx$, which is $\mu^h_0$, equals one.

**Theorem 1:** *If $q$ is odd, then $C_q(s)$, which is defined as follows, is invariant to blur in the wavelet domain with wavelet function $\psi(\cdot)$.*

$$C_q(s) = \acute{\mu}_q(s) - \frac{1}{\acute{\mu}_0(s)} \sum_{l=1}^{\frac{q-1}{2}} \frac{\binom{q}{q-2l}_{M_\psi}}{\binom{2l}{0}_{M_\psi}} C_{q-2l}(s)\, \acute{\mu}_{2l}(s) \tag{2.12}$$

PROOF When $q = 1$, $C_1^{\hat{g}^\psi}(s) = C_1^{\hat{f}^\psi}(s) = 0$.
For $q = 3$, it can be trivially shown that $C_3^{\hat{g}^\psi}(s) = C_3^{\hat{f}^\psi}(s)$.

$$\begin{aligned} C_3^{\hat{g}^\psi}(s) &= \acute{\mu}_3^{\hat{g}^\psi}(s) \\ &= \sum_{l=0}^{3} \binom{3}{l}_{M_\psi} \acute{\mu}_l^{\hat{f}^\psi}(s)\, \mu_{3-l}^h \\ &= \acute{\mu}_3^{\hat{f}^\psi}(s) = C_3^{\hat{f}^\psi}(s). \end{aligned} \tag{2.13}$$

If (2.12) is valid for $1, 3, ..., q-2$, it can be proved that it is valid for $q$ as well:

$$\begin{aligned} C_q^{\hat{g}^\psi}(s) &= \acute{\mu}_q^{\hat{g}^\psi}(s) - \frac{1}{\acute{\mu}_0^{\hat{g}^\psi}(s)} \sum_{l=1}^{\frac{q-1}{2}} \frac{\binom{q}{q-2l}_{M_\psi}}{\binom{2l}{0}_{M_\psi}} C_{q-2l}^{\hat{g}^\psi}(s)\, \acute{\mu}_{2l}^{\hat{g}^\psi}(s) \\ &= \sum_{k=0}^{q} \binom{q+M_\psi}{k} \acute{\mu}_{q-k}^{\hat{f}^\psi}(s) \mu_k^h \\ &- \frac{1}{\acute{\mu}_0^{\hat{f}^\psi}(s)} \sum_{l=1}^{\frac{q-1}{2}} \frac{\binom{q}{q-2l}_{M_\psi}}{\binom{2l}{0}_{M_\psi}} C_{q-2l}^{\hat{f}^\psi}(s) \sum_{k=0}^{2l} \binom{2l+M_\psi}{k} \acute{\mu}_{2l-k}^{\hat{f}^\psi}(s) \mu_k^h \\ &= C_q^{\hat{f}^\psi}(s) + \sum_{k=1}^{q} \binom{q+M_\psi}{k} \acute{\mu}_{q-k}^{\hat{f}^\psi}(s) \mu_k^h \\ &- \frac{1}{\acute{\mu}_0^{\hat{f}^\psi}(s)} \sum_{l=1}^{\frac{q-1}{2}} \frac{\binom{q}{q-2l}_{M_\psi}}{\binom{2l}{0}_{M_\psi}} C_{q-2l}^{\hat{f}^\psi}(s) \sum_{k=1}^{2l} \binom{2l+M_\psi}{k} \acute{\mu}_{2l-k}^{\hat{f}^\psi}(s) \mu_k^h \\ &= C_q^{\hat{f}^\psi}(s) + \sum_{k=1}^{q} \binom{q+M_\psi}{k} \acute{\mu}_{q-k}^{\hat{f}^\psi}(s) \mu_k^h \\ &- \frac{1}{\acute{\mu}_0^{\hat{f}^\psi}(s)} \sum_{l=1}^{\frac{q-1}{2}} \sum_{k=1}^{2l} \binom{2l+M_\psi}{k} \frac{\binom{q}{q-2l}_{M_\psi}}{\binom{2l}{0}_{M_\psi}} C_{q-2l}^{\hat{f}^\psi}(s)\, \acute{\mu}_{2l-k}^{\hat{f}^\psi}(s) \mu_k^h \\ &= C_q^{\hat{f}^\psi}(s) + \sum_{k=1}^{q} \binom{q+M_\psi}{k} \acute{\mu}_{q-k}^{\hat{f}^\psi}(s) \mu_k^h \\ &- \frac{1}{\acute{\mu}_0^{\hat{f}^\psi}(s)} \sum_{k=1}^{q-1} \sum_{l=[\frac{k+1}{2}]}^{\frac{q-1}{2}} \binom{q+M_\psi}{k} \frac{\binom{q-k}{q-2l}_{M_\psi}}{\binom{2l-k}{0}_{M_\psi}} C_{q-2l}^{\hat{f}^\psi}(s)\, \acute{\mu}_{2l-k}^{\hat{f}^\psi}(s) \mu_k^h \\ &= C_q^{\hat{f}^\psi}(s) + \binom{q+M_\psi}{q} \acute{\mu}_0^{\hat{f}^\psi}(s) \mu_q^h \sum_{k=1}^{q-1} \binom{q+M_\psi}{k} \mu_k^h \end{aligned}$$

$$\times \quad \left( \acute{\mu}^{\hat{f}^{\psi}}_{q-k}(s) - \frac{1}{\acute{\mu}^{\hat{f}^{\psi}}_{0}(s)} \sum_{l=[\frac{k+1}{2}]}^{\frac{q-1}{2}} \frac{\binom{q-k}{q-2l}_{M_\psi}}{\binom{2l-k}{0}_{M_\psi}} C^{\hat{f}^{\psi}}_{q-2l}(s)\, \acute{\mu}^{\hat{f}^{\psi}}_{2l-k}(s) \right)$$

$$= \quad C^{\hat{f}^{\psi}}_{q}(s) + \binom{q+M_\psi}{q} \acute{\mu}^{\hat{f}^{\psi}}_{0}(s) \mu^{h}_{q} + \sum_{k=1}^{q-1} \binom{q+M_\psi}{k} \mu^{h}_{k} J_{q,k}(s). \tag{2.14}$$

When $k$ is odd, $\mu^h_k$ is zero. Hence, the second term in (2.14) becomes zero. The only term in (2.14) that is dependent on the moments of $h$ is $J_{q,k}(s)$. In order to prove that the proposed invariant is independent of PSF, it is necessary to show that when $k$ is even, $J_{q,k}(s) = 0$ .

$$\begin{aligned}
J_{q,k}(s) &= \acute{\mu}^{\hat{f}^{\psi}}_{q-k}(s) - \frac{1}{\acute{\mu}^{\hat{f}^{\psi}}_{0}(s)} \sum_{l=\frac{k}{2}}^{\frac{q-1}{2}} \frac{\binom{q-k}{q-2l}_{M_\psi}}{\binom{2l-k}{0}_{M_\psi}} C^{\hat{f}^{\psi}}_{q-2l}(s)\, \acute{\mu}^{\hat{f}^{\psi}}_{2l-k}(s) \\
&= \acute{\mu}^{\hat{f}^{\psi}}_{q-k}(s) - \frac{1}{\acute{\mu}^{\hat{f}^{\psi}}_{0}(s)} \sum_{l=0}^{\frac{q-k-1}{2}} \frac{\binom{q-k}{q-k-2l}_{M_\psi}}{\binom{2l}{0}_{M_\psi}} C^{\hat{f}^{\psi}}_{q-k-2l}(s)\, \acute{\mu}^{\hat{f}^{\psi}}_{2l}(s) \\
&= \acute{\mu}^{\hat{f}^{\psi}}_{q-k}(s) - \frac{1}{\acute{\mu}^{\hat{f}^{\psi}}_{0}(s)} \sum_{l=1}^{\frac{q-k-1}{2}} \frac{\binom{q-k}{q-k-2l}_{M_\psi}}{\binom{2l}{0}_{M_\psi}} C^{\hat{f}^{\psi}}_{q-k-2l}(s)\, \acute{\mu}^{\hat{f}^{\psi}}_{2l}(s) \\
&- \frac{1}{\acute{\mu}^{\hat{f}^{\psi}}_{0}(s)} \frac{\binom{q-k}{q-k}_{M_\psi}}{\binom{0}{0}_{M_\psi}} C^{\hat{f}^{\psi}}_{q-k}(s)\, \acute{\mu}^{\hat{f}^{\psi}}_{0}(s) \\
&= C^{\hat{f}^{\psi}}_{q-k}(s) - C^{\hat{f}^{\psi}}_{q-k}(s) \\
&= 0.
\end{aligned} \tag{2.15}$$

Since $J_{q,k}(s)$ is zero when $k$ is odd, the only remaining term in (2.14) is $C^{\hat{f}^{\psi}}_{q}(s)$. Therefore, $C^{\hat{g}}_{q}(s) = C^{\hat{f}}_{q}(s)$. □

**Corollary 1:** *Flusser's invariants [16] are a special case of (2.12).*

PROOF To obtain Flusser's invariants, it is assumed that $\psi(\cdot)$ is the Dirac delta function. In this case, $M_\psi = 0$ which implies that $\psi(\cdot)$ is not a wavelet function anymore. Therefore, $p = q + M_\psi = q$ and $\mu_p = \acute{\mu}_q$. By setting $s = 1$ at all time, it is trivial to show that $\hat{f}^{\psi}(x, 1)$ is equivalent to $f(x)$, since the signal is convolved by the Dirac delta function. From here, (2.12) is rewritten with the new assumptions.

$$\begin{aligned}
C^{f}_{p} &= \mu_p - \frac{1}{\mu_0} \sum_{l=1}^{\frac{p-1}{2}} \frac{\binom{p}{p-2l}_{0}}{\binom{2l}{0}_{0}} C^{f}_{p-2l} \mu_{2l} \\
&= \mu_p - \frac{1}{\mu_0} \sum_{l=1}^{\frac{p-1}{2}} \binom{p}{p-2l} C^{f}_{p-2l} \mu_{2l}.
\end{aligned} \tag{2.16}$$

which is the definition of Flusser's blur invariants [16]. □

## 2.3 Experiment 1: Blur and Noise Analysis

In this section, the performance of the proposed invariants is demonstrated by applying it to 1D signals, and comparing to Flusser's invariants [16]. Two different types of wavelet functions were employed to demonstrate the performance of the invariants under the change of this parameter. The first wavelet function is Coiflet of order 1 ($M_\psi = 2$) [11]. There is no closed-form representation for this orthogonal wavelet. The second wavelet function belongs to the crude wavelet class. The wavelet function that is employed here is a hyperbolic kernel , which, unlike Coiflet, has an explicit expression (2.17). This wavelet function is comprehensively studied in [35, 36, 37], and different properties are extracted. For the experiments of this section, $n$ and $\beta$ were set to 4 and 1 respectively. This wavelet function has two vanishing moments as well.

$$\psi_{n,\beta}(x) = -n\beta^2 \operatorname{sech}^n(\beta x)\left(n - (n+1)\operatorname{sech}^2(\beta x)\right) \tag{2.17}$$

For this experiment, 1000 1D signals with the length of 200 and in the range of [-1 1] were artificially generated. Figure 2.1 shows one of the signals. The signals were blurred by calculating $N$-point neighbourhood averaging with a neighbourhood of 5, 7, 9, 11, 13, 15, 17, 19, 21, and 23. In order to study the effect of noise on the performance of the invariants, the signals were also contaminated with additive noise. The added noise was Gaussian with zero mean and the standard deviation of 0 (no noise), 0.001, 0.002, 0.008, 0.02, 0.04, and 0.08. The wavelet transform of the signals were obtained with the wavelet functions described above at 3 scales, $s = 2$, 4, and 8. The invariants for all of the original and blurred signals were calculated up to order 11 ($q = 9$, $p = q + M_\psi = 11$). However, the invariants of order 3 ($q = 1$, $p = q + M_\psi = 3$) are not reported since they are zero. Then, based on the following equation, the similarity between the original signals and their blurred versions was measured

$$R = \left| \frac{C_p^X - C_p^O}{C_p^O} \right| \tag{2.18}$$

where $C_p^O$ and $C_p^X$ are the $p^{th}$ order invariants of the actual and blurred signals respectively. The closer $C_p^X$ is to $C_p^O$, the smaller $R$ becomes.

Figures 2.2 and 2.3 show the medians of the similarity measures for invariants obtained with Coiflet and hyperbolic wavelet functions respectively. Both figures show invariants of three orders: 5, 7, and 9, and consists of 9 plots: 3 representing the results acquired with Flusser's invariants, and the other 6 results with the proposed invariants at two scales: 4 and 8. Every plot has several graphs representing different levels of noise. The $x-$axis represents the number of neighbourhoods in averaging, $N$, and the $y-$axis shows the similarity measure, $R$. The results acquired with Flusser's

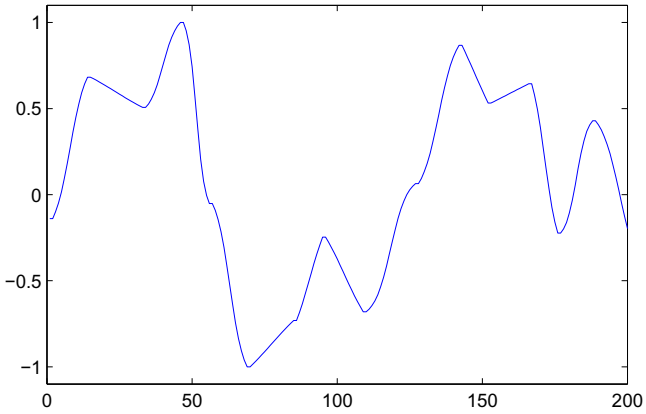


Figure 2.1: One of the artificial signals that was used in experiment I.

invariants are repeated in both figures for the sake of comparison. Also, Table 2.1 shows the eleventh order invariants of one the signals for different levels of noises.

The first noticeable property of the invariants is that by increasing the order of the invariants, $R$ increases as well. The reason of this rise is because the invariants also increase exponentially with respect to their order.

By changing the noise level, the similarity changes from 0% to 30% in Flusser's invariants and 25% in the wavelet based invariants, which is 5% less than the one in the spatial domain (Figures 2.2 and 2.3). The wavelet based invariants show a generally better robustness than Flusser's invariants in this experiment. However, it is impossible to make a general statement about the robustness of invariants in the wavelet domain than those in the spatial domain. The reason is that there are various wavelet functions available with different properties, which requires a comprehensive study of its own.

A slight increase in similarity is observable by the increase of $N$ in Flusser's invariants. It is also noticeable in the proposed invariants at scale 4, but it becomes less evident for the invariants at scale 8, specially for invariants with Coiflet. The similarity measure is also slightly less for these invariants. Since a higher scale is equivalent to a lower resolution, the effect of blur and noise is less significant. However, the risk of losing the properties of signals also increases. Therefore, a proper selection of scales is substantial.

Comparing the results obtained by Flusser's invariants and those of the wavelet based invariants indicates that the later is generally performing better. Employing different wavelet functions also

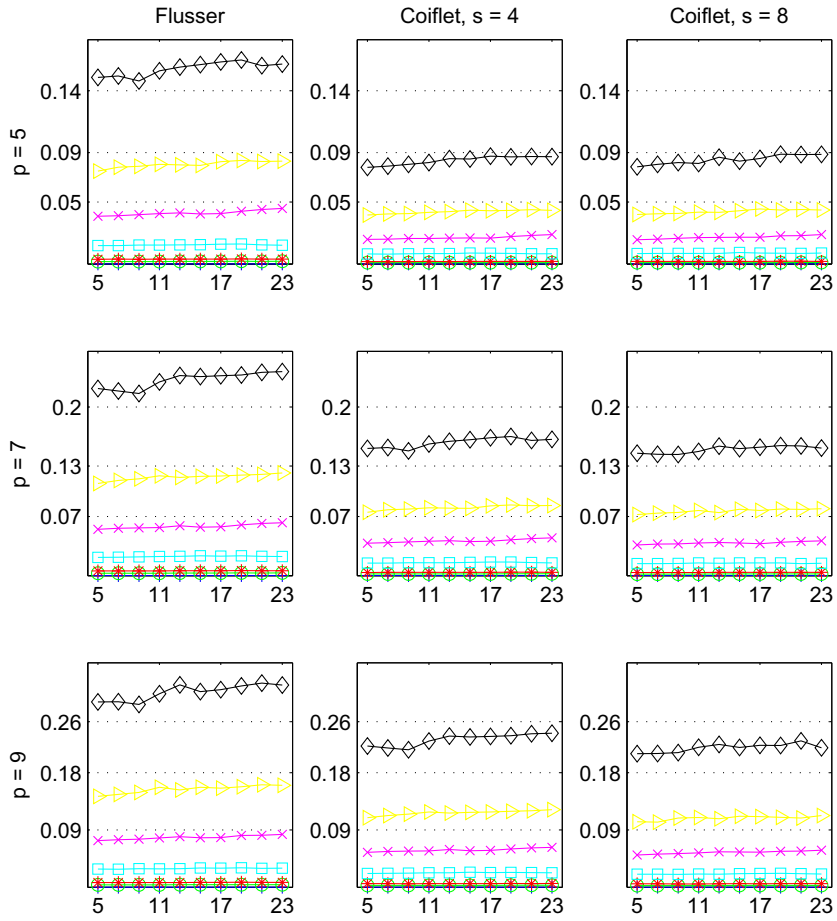


Figure 2.2: Median of similarity measures calculated for Flusser's invariants and the proposed invariants with Coiflet wavelet of order 1 at scales 4 and 8. Every plot shows the effect of different levels of noise. The $x$-axis represents $N$, which is the number of neighbourhood for averaging, and the $y$-axis shows the similarity measure $R$.

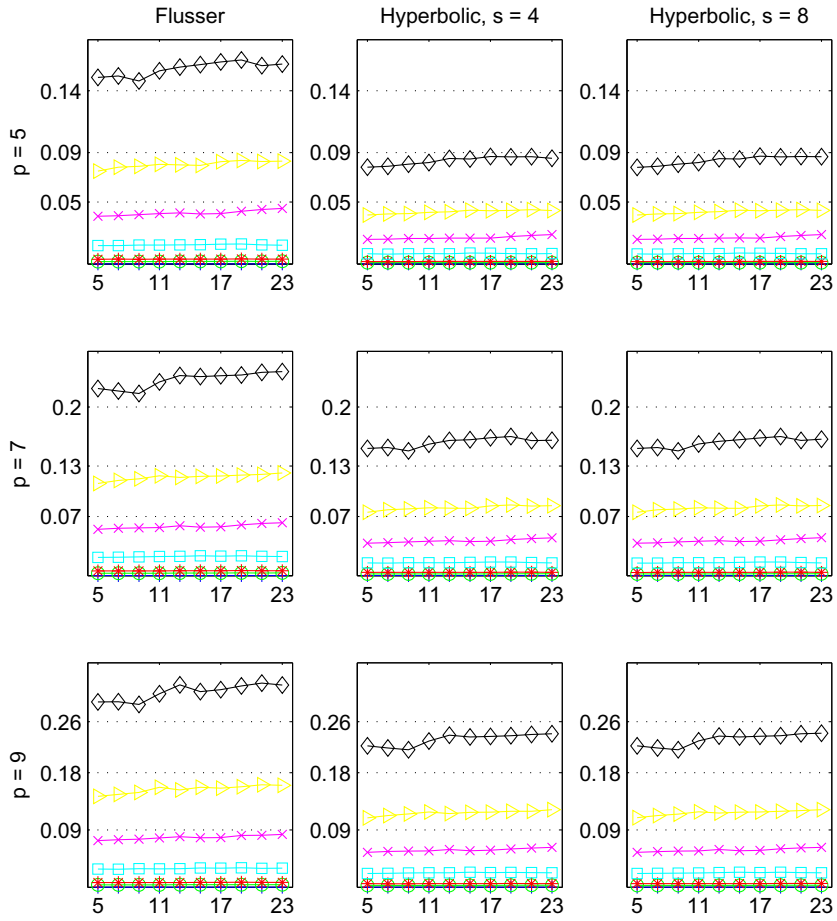


Figure 2.3: Median of similarity measures calculated for Flusser's invariants and the proposed invariants with Hyperbolic wavelet of order 4 at scales 4 and 8. Every plot shows the effect of different levels of noise. The $x$-axis represents $N$, which is the number of neighbourhood for averaging, and the $y$-axis shows the similarity measure $R$.

Table 2.1: Eleventh order invariants of an artificial signal that was used in experiment I. The invariants are shown for different levels of noise variances and two numbers of neighbourhoods in averaging. The scale, $s$, is 2.

| Noise | Flusser | | Coiflet ($s = 2$) | | Hyperbolic ($s = 2$) | |
|---|---|---|---|---|---|---|
| | $N$=7 | $N$=11 | $N$=7 | $N$=11 | $N$=7 | $N$=11 |
| 0.000 | -1.26e+31 | -1.26e+31 | 5.51e+30 | 5.51e+30 | 1.59e+32 | 1.59e+32 |
| 0.001 | -1.26e+31 | -1.26e+31 | 5.50e+30 | 5.50e+30 | 1.59e+32 | 1.59e+32 |
| 0.002 | -1.26e+31 | -1.27e+31 | 5.52e+30 | 5.53e+30 | 1.59e+32 | 1.60e+32 |
| 0.008 | -1.33e+31 | -1.32e+31 | 5.79e+30 | 5.74e+30 | 1.69e+32 | 1.68e+32 |
| 0.020 | -1.12e+31 | -1.13e+31 | 4.88e+30 | 4.92e+30 | 1.37e+32 | 1.38e+32 |
| 0.040 | -1.59e+31 | -1.57e+31 | 6.92e+30 | 6.84e+30 | 2.12e+32 | 2.09e+32 |
| 0.080 | -9.81e+30 | -9.81e+30 | 4.28e+30 | 4.28e+30 | 1.16e+32 | 1.16e+32 |

did not have any major influence on the performance of the invariants, but provide a different range of values (Table 2.1). As it is mentioned above, it is possible that with a different choice of wavelet function contrary results would be obtained. The application that the proposed invariants are supposed to be used could have a significant influence on the choice of the wavelet function, since different types of wavelet functions are sensitive to different properties in signals [46]. It might be even useful to employ multiple wavelet functions in order to extract different moment invariants for a comprehensive analysis.

## 2.4 Blur Invariants for 1D Discrete Signals

DWT is the common appraoch for wavelet decomposition of discrete signals. However, this tool is not shift invariant. In order to preserve the shift invariance property, the *à trous* algorithm (eq. 1.10 and 1.11) is used. Also, the moment definitions for discrete signals (1.26 - 1.28) are employed in this section. Having chosen the proper wavelet transform, the representation of blur and moments in the wavelet domain will be extracted.

### 2.4.1 Blur in the Wavelet Domain for 1D Discrete Signals

The wavelet transform of a blurred signal with wavelet function $\psi_L$ is

$$\overset{\psi_L}{W}y[n] = \bar{\psi}_L \star y[n], \tag{2.19}$$

where $y[n] = b \star x[n]$, is a discrete representation of (2.2), with $b$ as the blur system, and $x$ as the original signal. Substituting $y$ with its equivalent gives

$$\begin{aligned}\overset{\psi_L}{W}y[n] &= \bar{\psi}_L \star b \star x[n] \\ &= b \star \bar{\psi}_L \star x[n] = b \star \overset{\psi_L}{W}x[n].\end{aligned} \tag{2.20}$$

Eq. (2.20) implies that the wavelet transform of blurred signal $y$ is the convolution of blur system $b$ with the wavelet transform of original signal $x$.

### 2.4.2 Moments in the Wavelet Domain for 1D Discrete Signals

The ordinary moment of order $p$ of $\overset{\psi_L}{W}x$ is

$$\begin{aligned}m_p^{\overset{\psi_L}{W}x} &= \sum_n n^p \overset{\psi_L}{W}x[n] \\ &= \sum_n \sum_l n^p x[l]\psi_L[l-n] = \sum_l \sum_k (l-k)^p x[l]\psi_L[k] \\ &= \sum_{i=0}^{p} \sum_l \sum_k \binom{p}{i} (-1)^i l^{p-i} x[l]k^i \psi_L[k] = \sum_{i=0}^{p} \binom{p}{i} (-1)^i m_{p-i}^x m_i^{\psi_L},\end{aligned} \tag{2.21}$$

where $l-n$ is substituted with $k$. If $\psi_L$ has $M_{\psi_L}$ vanishing moments, $m_i^{\psi_L}$ in (2.21) will be zero for $i < M_{\psi_L}$. This forces the moments of $\overset{\psi_L}{W}x$ to also be zero for $p < M_{\psi_L}$. Considering this and similar to the case for continuous signals, the generalized definition of centroid (eq. 2.9) can be used in (1.28) to overcome this problem. Therefore, the central moment of order $p$ of $\overset{\psi_L}{W}y$ is

$$\begin{aligned}\mu_p^{\overset{\psi_L}{W}y} &= \sum_n \left(n - \varsigma^{\overset{\psi_L}{W}y}\right)^p \overset{\psi_L}{W}y[n] = \sum_n \sum_l \left(n - \varsigma^{\overset{\psi_L}{W}y}\right)^p \overset{\psi_L}{W}x[l]b[n-l] \\ &= \sum_l \sum_k \left(\left(l - \varsigma^{\overset{\psi_L}{W}x}\right) + \left(k - c^b\right)\right)^p \overset{\psi_L}{W}x[l]b[k] \\ &= \sum_{i=0}^{p} \sum_l \sum_k \binom{p}{i} \left(l - \varsigma^{\overset{\psi_L}{W}x}\right)^i \overset{\psi_L}{W}x[l] \left(k - c^b\right)^{p-i} b[k] \\ &= \sum_{i=0}^{p} \binom{p}{i} \mu_i^{\overset{\psi_L}{W}x} \mu_{p-i}^b,\end{aligned} \tag{2.22}$$

where $l-n$ is substituted with $k$. Also, it is trivial to show that $\overset{\psi_L}{\varsigma^{Wy}} = \overset{\psi_L}{\varsigma^{Wx}} + c^b$. Since $\overset{\psi_L}{\mu_i^{Wx}}$ is zero for $i < M_{\psi_L}$, $p$ should be equal to or greater than $M_{\psi_L}$. Therefore, by defining $q + M_{\psi_L} = p$, $\acute{\mu}_q = \mu_p$, and $\binom{a}{b}_M = \binom{a+M}{b+M}$, (2.22) is modified to

$$\overset{\psi_L}{\acute{\mu}_q^{Wy}} = \sum_{i=0}^{q} \binom{q}{i}_{M_{\psi_L}} \overset{\psi_L}{\acute{\mu}_i^{Wx}} \mu_{q-i}^b. \tag{2.23}$$

### 2.4.3 Wavelet Domain Blur Invariants for 1D Discrete Signals

It is clear from (2.23) that the central moments of a blurred signal are related to those of the original signal and the blur system. To have wavelet domain blur invariants based on these moments, it is required to find a combination of them such that the moments of the blur system are not present any longer.

**Theorem 2:** *For $\overset{\psi_L}{Wx}$, which is the wavelet transform of $x$ with wavelet function $\psi_L$, $\overset{\psi_L}{C_q^{Wx}}$ is invariant to symmetric and energy-preserving blur systems.*

$$\overset{\psi_L}{C_q^{Wx}} = \begin{cases} \overset{\psi_L}{\acute{\mu}_q^{Wx}} - \dfrac{1}{\overset{\psi_L}{\acute{\mu}_0^{Wx}}} \displaystyle\sum_{l=0}^{\frac{q-1}{2}} \frac{\binom{q}{q-2l}_{M_{\psi_L}}}{\binom{2l}{0}_{M_{\psi_L}}} \overset{\psi_L}{C_{q-2l}^{Wx}} \overset{\psi_L}{\acute{\mu}_{2l}^{Wx}}, & l \text{ is odd} \\ 0, & l \text{ is even.} \end{cases} \tag{2.24}$$

PROOF Refer to the proof of Theorem 1. □

Theorem 2 is applicable when the blur system is energy-preserving. However, such systems are not always realistic. The next theorem eliminates this restriction.

**Theorem 3:** *For $\overset{\psi_L}{Wx}$, which is the wavelet transform of $x$ with wavelet function $\psi_L$, $\overset{\psi_L}{D_q^{Wx}}$ is invariant to symmetric blur systems.*

$$\overset{\psi_L}{D_q^{Wx}} = \begin{cases} \overset{\psi_L}{\acute{\nu}_q^{Wx}} - \displaystyle\sum_{l=0}^{\frac{q-1}{2}} \frac{\binom{q}{q-2l}_{M_{\psi_L}}}{\binom{2l}{0}_{M_{\psi_L}}} \overset{\psi_L}{D_{q-2l}^{Wx}} \overset{\psi_L}{\acute{\nu}_{2l}^{Wx}}, & l \text{ is odd} \\ 0, & l \text{ is even,} \end{cases} \tag{2.25}$$

*where $\acute{\nu}_q^x = \acute{\mu}_q^x / \acute{\mu}_0^x$.*

PROOF Assume $\tilde{b}$ is a non-energy-preserving system. Such systems could be represented as

$$\tilde{b} = cb, \tag{2.26}$$

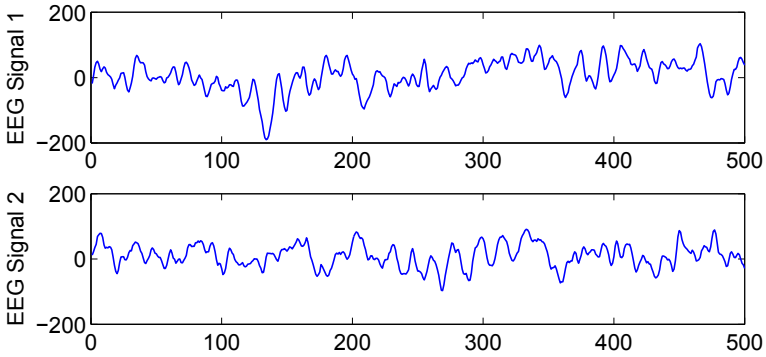


Figure 2.4: The two EEG signals that are used in experiment 1.

where $c$ and $b$ are a constant and an energy-preserving system, respectively. It is trivial to show that $\mu_q^{\tilde{b}} = c\mu_q^b$, and from here $c$ can be found as the zero order moment of the non-energy-preserving system, $\mu_0^{\tilde{b}}$. Remember that the zero order moment of an energy-preserving system is equal to 1.

Assuming that $y$ and $z$ are both blurred versions of $x$ by blur systems $\tilde{b}$ and $b$, respectively, it can trivially be shown that $\acute{\nu}^{\overset{\psi}{W}_L y} = \acute{\nu}^{\overset{\psi}{W}_L z}$.

Without loss of generality, $\nu$ can be replaced in (2.24) to achieve blur invariants with no restriction on the energy of the system, given in (2.25). It should also be mention that since $\nu_0^{\overset{\psi}{W}_L x}$ becomes 1 for all signals, the term before the summation in (2.24) does not appear in (2.25) any more. □

## 2.5 Experiment 2: Blur Analysis

In this section, the blur invariants are evaluated in an experiment with blurred EEG signals. Wavelet function Daubechies of order 2 (DB2), which has 2 vanishing moments [11], is used in this experiment, and is carried out at level $ghh$, which means that the wavelet transform of the signals is obtained by applying the highpass filter followed twice by the lowpass filter.

Figure 2.4 shows the two EEG signals that are used for this experiment. They are chosen from the database generated by Andrzejak et al. [2]. The signals are blurred by averaging on $N$ neighbourhoods, where $N$ is 11 and 21, and energies of 0.7 and 0.4, respectively.

Table 2.2 represents the invariants of order 5 to 11 of the original signals and their blurred ones. It is clear that blur intensity and system energy changes do not affect the invariants significantly. Also, the two different signals can be perfectly distinguished from each other using the invariants.

Table 2.2: Invariants of the EEG signals degraded with different blur systems. The wavelet filter is Daubechies of order two at level $ghh$. O.M. stands for the order of magnitude of the blur invariants. $N$ is the number of neighbourhoods in averaging. $N = 0$ refers to the original signal.

| | $q$/O.M. | 5/7 | 7/13 | 9/19 | 11/25 |
|---|---|---|---|---|---|
| | $N/m_0^{\tilde{b}}$ | | | | |
| Sig. 1 | 0 | 56.49 | 130.22 | 617.55 | 4317.66 |
| | 11/0.7 | 56.48 | 130.18 | 617.25 | 4314.94 |
| | 21/0.4 | 56.53 | 130.44 | 618.98 | 4330.91 |
| Sig. 2 | 0 | -0.41 | 0.21 | -0.16 | 0.19 |
| | 11/0.7 | -0.41 | 0.20 | -0.16 | 0.19 |
| | 21/0.4 | -0.40 | 0.20 | -0.16 | 0.18 |

## 2.6 Blur Invariants for 2D Discrete Signals

Similar to the case for 1D discrete signals in order to preserve the shift invariance property, it is required to use the *à trous* algorithm (eq. 1.14 - 1.17). Also, the moment definitions for discrete signals (eq. 1.29 - 1.31) are employed in this section.

### 2.6.1 Blur in the Wavelet Domain for 2D Discrete Signals

The representation of (2.2) for 2D discrete signals is

$$y[n_1, n_2] = b \star x[n_1, n_2], \tag{2.27}$$

were $y$ and $x$ are the blurred and original signals, respectively, and $b$ models the blur system. The wavelet transform of a blurred signal with wavelet function $\psi_L$ is

$$\overset{\psi_L}{W} y[n_1, n_2] = \bar{\psi}_L \star y[n_1, n_2]. \tag{2.28}$$

Substituting $y$ with its equivalent in (2.27) gives

$$\begin{aligned} \overset{\psi_L}{W} y[n_1, n_2] &= \bar{\psi}_L \star b \star x[n_1, n_2] \\ &= b \star \bar{\psi}_L \star x[n_1, n_2] \\ &= b \star \overset{\psi_L}{W} x[n_1, n_2]. \end{aligned} \tag{2.29}$$

Eq. (2.29) implies that the wavelet transform of blurred signal $y$ is the convolution of blur system $b$ with the wavelet transform of original signal $x$.

### 2.6.2 Moments in the Wavelet Domain for 2D Discrete Signals

The ordinary moment of order $(p+q)$ of $\overset{\psi_L}{W}x$ is

$$\begin{aligned}
m_{p,q}^{\overset{\psi_L}{W}x} &= \sum_{n_1}\sum_{n_2} n_1^p n_2^q \overset{\psi_L}{W}x[n_1,n_2] \\
&= \sum_{n_1}\sum_{n_2}\sum_{n_3}\sum_{n_4} n_1^p n_2^q x[n_3,n_4]\psi_L[n_3-n_1,n_4-n_2] \\
&= \sum_{n_3}\sum_{n_4}\sum_{n_5}\sum_{n_6} (n_3-n_5)^p (n_4-n_6)^q x[n_3,n_4]\psi_L[n_5,n_6] \\
&= \sum_{i=0}^{p}\sum_{j=0}^{q}\sum_{n_3}\sum_{n_4}\sum_{n_5}\sum_{n_6}\binom{p}{i}\binom{q}{j}(-1)^{i+j} n_3^{p-i} n_4^{q-j} x[n_3,n_4] n_5^i n_6^j \psi_L[n_5,n_6] \\
&= \sum_{i=0}^{p}\sum_{j=0}^{q}\binom{p}{i}\binom{q}{j}(-1)^{i+j} m_{p-i,q-j}^{x} m_{i,j}^{\psi_L}, \qquad (2.30)
\end{aligned}$$

where $n_3-n_1$ and $n_4-n_2$ are substituted with $n_4$ and $n_5$, respectively. If $\psi_L$ has $M_{\psi_L^1}$ and $M_{\psi_L^2}$ vanishing moments on the first and second dimensions, respectively, $m_{i,j}^{\psi_L}$ in (2.30) will be zero if $i<M_{\psi_L^1}$ or $j<M_{\psi_L^2}$. This forces the moments of $\overset{\psi_L}{W}x$ to also be zero if $p<M_{\psi_L^1}$ or $q<M_{\psi_L^2}$, therefore it is not possible to use the original definition of centroid (eq. 1.30) for this type of signals. It is, however, possible to extend the generalized definition of centroid for 2D signals as well.

**Definition 2.** *If the moments of $x$ are zero up to order $M_1-1$ and $M_2-1$ on the first and second dimensions, respectively, its centroid is defined as*

$$\varsigma_1^x = \frac{m_{M_1+1,M_2}^x}{(M_1+1)m_{M_1,M_2}^x}\,,\ \varsigma_2^x = \frac{m_{M_1,M_2+1}^x}{(M_2+1)m_{M_1,M_2}^x}. \qquad (2.31)$$

If $M_1$ and $M_2$ are zero, then it is easy to show that $\varsigma_1^x$ and $\varsigma_2^x$ would become $c_1^x$ and $c_2^x$, respectively. By simply substituting $c_1^x$ and $c_2^x$ in (1.31) with $\varsigma_1^x$ and $\varsigma_2^x$, the central moments of the wavelet transform of signals can be calculated. Therefore, the central moment of order $(p+q)$ of $\overset{\psi_L}{W}y$ is

$$\begin{aligned}
\mu_{p,q}^{\overset{\psi_L}{W}y} &= \sum_{n_1}\sum_{n_2}\left(n_1-\varsigma_1^{\overset{\psi_L}{W}y}\right)^p\left(n_2-\varsigma_2^{\overset{\psi_L}{W}y}\right)^q \overset{\psi_L}{W}y[n_1,n_2] \\
&= \sum_{n_1}\sum_{n_2}\sum_{n_3}\sum_{n_4}\left(n_1-\varsigma_1^{\overset{\psi_L}{W}y}\right)^p\left(n_2-\varsigma_2^{\overset{\psi_L}{W}y}\right)^q \overset{\psi_L}{W}x[n_3,n_4]b[n_1-n_3,n_2-n_4] \\
&= \sum_{n_3}\sum_{n_4}\sum_{n_5}\sum_{n_6}\left(\left(n_3-\varsigma_1^{\overset{\psi_L}{W}x}\right)+\left(n_5-c_1^b\right)\right)^p\left(\left(n_4-\varsigma_2^{\overset{\psi_L}{W}x}\right)+\left(n_6-c_2^b\right)\right)^q \\
&\quad\times \overset{\psi_L}{W}x[n_3,n_4]b[n_5,n_6] \\
&= \sum_{i=0}^{p}\sum_{j=0}^{q}\sum_{n_3}\sum_{n_4}\sum_{n_5}\sum_{n_6}\binom{p}{i}\binom{q}{j}\left(n_3-\varsigma_1^{\overset{\psi_L}{W}x}\right)^i\left(n_4-\varsigma_2^{\overset{\psi_L}{W}x}\right)^j \overset{\psi_L}{W}x[n_3,n_4]
\end{aligned}$$

$$\times \left(n_5 - c_1^b\right)^{p-i} \left(n_6 - c_2^b\right)^{q-j} b[n_5, n_6]$$
$$= \sum_{i=0}^{p}\sum_{j=0}^{q} \binom{p}{i}\binom{q}{j} \mu_{i,j}^{\overset{\psi_L}{Wx}} \mu_{p-i,q-j}^{b}, \tag{2.32}$$

where $n_3 - n_1$ and $n_4 - n_2$ are substituted with $n_4$ and $n_5$, respectively. Also, it is trivial to show that $\varsigma_i^{\overset{\psi_L}{Wy}} = \varsigma_i^{\overset{\psi_L}{Wx}} + c_i^b$, where $i = 1, 2$. Since $\mu_{i,j}^{\overset{\psi_L}{Wx}}$ is zero for $i < M_{\psi_L^1}$ or $j < M_{\psi_L^2}$, $p$ and $q$ should be equal to or greater than $M_{\psi_L^1}$ and $M_{\psi_L^2}$, respectively. Therefore, by defining $r + M_{\psi_L^1} = p$, $s + M_{\psi_L^2} = q$, $\acute{\mu}_{r,s} = \mu_{p,q}$, and $\binom{a}{b}_M = \binom{a+M}{b+M}$, (2.32) is modified to

$$\acute{\mu}_{r,s}^{\overset{\psi_L}{Wy}} = \sum_{i=0}^{r}\sum_{j=0}^{s} \binom{r}{i}_{M_{\psi_L^1}} \binom{s}{j}_{M_{\psi_L^2}} \acute{\mu}_{i,j}^{\overset{\psi_L}{Wx}} \mu_{r-i,s-j}^{b}. \tag{2.33}$$

### 2.6.3 Wavelet Domain Blur Invariants for 2D Discrete Signals

Based on (2.33), the central moments of the blurred signal depend on the central moments of the original signal and the blur system. In order to have blur invariant descriptors based on the central moments, it is required to extract a combination of them in which the moments of the blur system are not present any longer. The blur system is assumed to be centrally symmetric, which is a general format for different blur systems, e.g. defocus, atmosphere turbulence, linear motion,

$$b\left[n_1, n_2\right] = b\left[-n_1, -n_2\right]. \tag{2.34}$$

The odd moments of such systems are zero. This property is exploited in order to extract blur invariant descriptors.

**Theorem 4:** *For $\overset{\psi_L}{W}x$, which is the wavelet transform of $x \in \mathbf{L^1}(\mathbb{Z}^2)$ with wavelet function $\psi_L \in \mathbf{L^2}(\mathbb{Z}^2)$, $C_{r,s}^{\overset{\psi_L}{Wx}}$ is invariant to centrally symmetric and energy-preserving blur operators.*

$$C_{r,s}^{\overset{\psi_L}{Wx}} = \begin{cases} \acute{\mu}_{r,s}^{\overset{\psi_L}{Wx}} - \dfrac{1}{\acute{\mu}_{0,0}^{\overset{\psi_L}{Wx}}} \underbrace{\sum_{i=0}^{r}\sum_{j=0}^{s}}_{0<i+j<r+s} \dfrac{\binom{r}{r-i}_{M_{\psi_L^1}} \binom{s}{s-j}_{M_{\psi_L^2}}}{\binom{i}{0}_{M_{\psi_L^1}} \binom{j}{0}_{M_{\psi_L^2}}} C_{r-i,s-j}^{\overset{\psi_L}{Wx}} \acute{\mu}_{i,j}^{\overset{\psi_L}{Wx}}, & (r+s)\ odd \\ 0, & (r+s)\ even. \end{cases} \tag{2.35}$$

Proof It is trivial to show that (2.35) holds for $(r + s) = 1, 3$. When $r = 1, s = 0$ or $r = 0, s = 1$, then $C_{1,0}^{\overset{\psi_L}{Wy}} = C_{0,1}^{\overset{\psi_L}{Wy}} = C_{1,0}^{\overset{\psi_L}{Wy}} = C_{0,1}^{\overset{\psi_L}{Wy}} = 0$.

When $r = 3, s = 0$,

$$C_{3,0}^{\overset{\psi_L}{Wy}} = \acute{\mu}_{3,0}^{\overset{\psi_L}{Wy}}$$

$$= \sum_{i=0}^{3}\sum_{j=0}^{0} \binom{3}{i}_{M_{\psi_L^1}} \binom{0}{j}_{M_{\psi_L^2}} \acute{\mu}_{i,j}^{\overset{\psi_L}{Wx}} \mu_{3-i,0-j}^{b}$$
$$= \acute{\mu}_{3,0}^{\overset{\psi_L}{Wx}} = C_{3,0}^{\overset{\psi_L}{Wx}}. \tag{2.36}$$

It also holds for $r = 0, s = 3$.

When $r = 2, s = 1$,

$$C_{2,1}^{\overset{\psi_L}{Wy}} = \acute{\mu}_{2,1}^{\overset{\psi_L}{Wy}}$$
$$= \sum_{i=0}^{2}\sum_{j=0}^{1} \binom{2}{i}_{M_{\psi_L^1}} \binom{1}{j}_{M_{\psi_L^2}} \acute{\mu}_{i,j}^{\overset{\psi_L}{Wx}} \mu_{2-i,1-j}^{b}$$
$$= \acute{\mu}_{2,1}^{\overset{\psi_L}{Wx}} = C_{2,1}^{\overset{\psi_L}{Wx}}. \tag{2.37}$$

The same holds for $r = 1, s = 2$.

In order to show that (2.35) is invariant to blur for all of the orders, it is required to employ a different representation of (2.33),

$$\acute{\mu}_{r,s}^{\overset{\psi_L}{Wy}} = \sum_{k=0}^{r}\sum_{l=0}^{s} \binom{r + M_{\psi_L^1}}{k} \binom{s + M_{\psi_L^2}}{l} \acute{\mu}_{r-k,s-l}^{\overset{\psi_L}{Wx}} \mu_{k,l}^{b}. \tag{2.38}$$

If (2.35) is valid for $(r + s) = 1, 2, \cdots, O - 2$, where $O$ is odd, it can be proved that it is also valid for $(r + s) = O$.

$$C_{r,s}^{\overset{\psi_L}{Wy}} = \acute{\mu}_{r,s}^{\overset{\psi_L}{Wy}} - \frac{1}{\acute{\mu}_{0,0}^{\overset{\psi_L}{Wy}}} \underbrace{\sum_{i=0}^{r}\sum_{j=0}^{s}}_{0<i+j<r+s} \frac{\binom{r}{r-i}_{M_{\psi_L^1}} \binom{s}{s-j}_{M_{\psi_L^2}}}{\binom{i}{0}_{M_{\psi_L^1}} \binom{j}{0}_{M_{\psi_L^2}}} C_{r-i,s-j}^{\overset{\psi_L}{Wy}} \acute{\mu}_{i,j}^{\overset{\psi_L}{Wy}}$$
$$= \sum_{k=0}^{r}\sum_{l=0}^{s} \binom{r + M_{\psi_L^1}}{k} \binom{s + M_{\psi_L^2}}{l} \acute{\mu}_{r-k,s-l}^{\overset{\psi_L}{Wx}} \mu_{k,l}^{b}$$
$$- \frac{1}{\acute{\mu}_{0,0}^{\overset{\psi_L}{Wx}}} \underbrace{\sum_{i=0}^{r}\sum_{j=0}^{s}}_{0<i+j<r+s} \frac{\binom{r}{r-i}_{M_{\psi_L^1}} \binom{s}{s-j}_{M_{\psi_L^2}}}{\binom{i}{0}_{M_{\psi_L^1}} \binom{j}{0}_{M_{\psi_L^2}}} C_{r-i,s-j}^{\overset{\psi_L}{Wx}} \sum_{k=0}^{i}\sum_{l=0}^{j} \binom{i + M_{\psi_L^1}}{l} \binom{j + M_{\psi_L^2}}{k} \acute{\mu}_{i-k,j-l}^{\overset{\psi_L}{Wx}} \mu_{k,l}^{b}$$
$$= C_{r,s}^{\overset{\psi_L}{Wx}} + \underbrace{\sum_{k=0}^{r}\sum_{l=0}^{s}}_{0<k+l} \binom{r + M_{\psi_L^1}}{k} \binom{s + M_{\psi_L^2}}{l} \acute{\mu}_{r-k,s-l}^{\overset{\psi_L}{Wx}} \mu_{k,l}^{b}$$
$$- \frac{1}{\acute{\mu}_{0,0}^{\overset{\psi_L}{Wx}}} \underbrace{\sum_{i=0}^{r}\sum_{j=0}^{s}}_{0<i+j<r+s} \frac{\binom{r}{r-i}_{M_{\psi_L^1}} \binom{s}{s-j}_{M_{\psi_L^2}}}{\binom{i}{0}_{M_{\psi_L^1}} \binom{j}{0}_{M_{\psi_L^2}}} C_{r-i,s-j}^{\overset{\psi_L}{Wx}} \underbrace{\sum_{k=0}^{i}\sum_{l=0}^{j}}_{0<k+l} \binom{i + M_{\psi_L^1}}{l} \binom{j + M_{\psi_L^2}}{k} \acute{\mu}_{i-k,j-l}^{\overset{\psi_L}{Wx}} \mu_{k,l}^{b}$$

$$
\begin{aligned}
&= C_{r,s}^{\overset{\psi_L}{Wx}} + \underbrace{\sum_{k=0}^{r}\sum_{l=0}^{s}}_{0<k+l}\binom{r+M_{\psi_L^1}}{k}\binom{s+M_{\psi_L^2}}{l}\acute{\mu}_{r-k,s-l}^{\overset{\psi_L}{Wx}}\mu_{k,l}^{b} \\
&- \frac{1}{\acute{\mu}_{0,0}^{\overset{\psi_L}{Wx}}}\underbrace{\sum_{i=0}^{r}\sum_{j=0}^{s}}_{0<i+j<r+s}\underbrace{\sum_{k=0}^{i}\sum_{l=0}^{j}}_{0<k+l}\frac{\binom{r}{r-i}_{M_{\psi_L^1}}\binom{i+M_{\psi_L^1}}{l}\binom{s}{s-j}_{M_{\psi_L^2}}\binom{j+M_{\psi_L^2}}{k}}{\binom{i}{0}_{M_{\psi_L^1}}\binom{j}{0}_{M_{\psi_L^2}}}C_{r-i,s-j}^{\overset{\psi_L}{Wx}}\acute{\mu}_{i-k,j-l}^{\overset{\psi_L}{Wx}}\mu_{k,l}^{b} \\
&= C_{r,s}^{\overset{\psi_L}{Wx}} + \underbrace{\sum_{k=0}^{r}\sum_{l=0}^{s}}_{0<k+l}\binom{r+M_{\psi_L^1}}{k}\binom{s+M_{\psi_L^2}}{l}\acute{\mu}_{r-k,s-l}^{\overset{\psi_L}{Wx}}\mu_{k,l}^{b} \\
&- \frac{1}{\acute{\mu}_{0,0}^{\overset{\psi_L}{Wx}}}\underbrace{\sum_{k=0}^{r}\sum_{l=0}^{s}}_{0<k+l}\underbrace{\sum_{i=l}^{r}\sum_{j=k}^{s}}_{i+j<r+s}\binom{r+M_{\psi_L^1}}{k}\binom{s+M_{\psi_L^2}}{l}\mu_{k,l}^{b}\frac{\binom{r-k}{r-i}_{M_{\psi_L^1}}\binom{t-l}{s-j}_{M_{\psi_L^2}}}{\binom{i-k}{0}_{M_{\psi_L^1}}\binom{j-l}{0}_{M_{\psi_L^2}}}C_{r-i,s-j}^{\overset{\psi_L}{Wx}}\acute{\mu}_{i-k,j-l}^{\overset{\psi_L}{Wx}} \\
&= C_{r,s}^{\overset{\psi_L}{Wx}} + \underbrace{\sum_{k=0}^{r}\sum_{l=0}^{s}}_{0<k+l}\binom{r+M_{\psi_L^1}}{k}\binom{s+M_{\psi_L^2}}{l}\mu_{k,l}^{b} \\
&\times\left(\acute{\mu}_{r-k,s-l}^{\overset{\psi_L}{Wx}} - \frac{1}{\acute{\mu}_{0,0}^{\overset{\psi_L}{Wx}}}\underbrace{\sum_{i=l}^{r}\sum_{j=k}^{s}}_{i+j<r+s}\frac{\binom{r-k}{r-i}_{M_{\psi_L^1}}\binom{t-l}{s-j}_{M_{\psi_L^2}}}{\binom{i-k}{0}_{M_{\psi_L^1}}\binom{j-l}{0}_{M_{\psi_L^2}}}C_{r-i,s-j}^{\overset{\psi_L}{Wx}}\acute{\mu}_{i-k,j-l}^{\overset{\psi_L}{Wx}}\right) \\
&= C_{r,s}^{\overset{\psi_L}{Wx}} + \underbrace{\sum_{k=0}^{r}\sum_{l=0}^{s}}_{0<k+l}\binom{r+M_{\psi_L^1}}{k}\binom{s+M_{\psi_L^2}}{l}\mu_{k,l}^{b}J_{r-k,s-l}. \qquad (2.39)
\end{aligned}
$$

In order to prove that $C_{r,s}^{\overset{\psi_L}{Wy}} = C_{r,s}^{\overset{\psi_L}{Wx}}$, it is required to prove that the second term in (2.39) is equal to zero. Since it is assumed that the blur operator is centrally symmetric, $\mu_{k,l}^{b}$ is zero when $(k+l)$ is odd. Therefore, it is only required to show that $J_{r-k,s-l}$ is zero for even orders.

$$
\begin{aligned}
J_{r-k,s-l} &= \acute{\mu}_{r-k,s-l}^{\overset{\psi_L}{Wx}} - \frac{1}{\acute{\mu}_{0,0}^{\overset{\psi_L}{Wx}}}\underbrace{\sum_{i=l}^{r}\sum_{j=k}^{s}}_{i+j<r+s}\frac{\binom{r-k}{r-i}_{M_{\psi_L^1}}\binom{s-l}{s-j}_{M_{\psi_L^2}}}{\binom{i-k}{0}_{M_{\psi_L^1}}\binom{j-l}{0}_{M_{\psi_L^2}}}C_{r-i,s-j}^{\overset{\psi_L}{Wx}}\acute{\mu}_{i-k,j-l}^{\overset{\psi_L}{Wx}} \\
&= \acute{\mu}_{r-k,s-l}^{\overset{\psi_L}{Wx}} - \frac{1}{\acute{\mu}_{0,0}^{\overset{\psi_L}{Wx}}}\underbrace{\sum_{i=0}^{r-k}\sum_{j=0}^{s-l}}_{i+j<r+s-k-l}\frac{\binom{r-k}{r-k-i}_{M_{\psi_L^1}}\binom{s-l}{s-l-j}_{M_{\psi_L^2}}}{\binom{i}{0}_{M_{\psi_L^1}}\binom{j}{0}_{M_{\psi_L^2}}}C_{r-i-k,s-j-l}^{\overset{\psi_L}{Wx}}\acute{\mu}_{i,j}^{\overset{\psi_L}{Wx}}
\end{aligned}
$$

$$
\begin{aligned}
&= \acute{\mu}^{\overset{\psi_L}{Wx}}_{r-k,s-l} - \frac{1}{\acute{\mu}^{\overset{\psi_L}{Wx}}_{0,0}} \underbrace{\sum_{i=0}^{r-k}\sum_{j=0}^{s-l}}_{0<i+j<r+s-k-l} \frac{\binom{r-k}{r-k-i}_{M_{\psi_L^1}} \binom{s-l}{s-l-j}_{M_{\psi_L^2}}}{\binom{i}{0}_{M_{\psi_L^1}} \binom{j}{0}_{M_{\psi_L^2}}} C^{\overset{\psi_L}{Wx}}_{r-i-k,s-j-l} \acute{\mu}^{\overset{\psi_L}{Wx}}_{i,j} \\
&- \frac{1}{\acute{\mu}^{\overset{\psi_L}{Wx}}_{0,0}} \frac{\binom{r-k}{r-k}_{M_{\psi_L^1}} \binom{s-l}{s-l}_{M_{\psi_L^2}}}{\binom{0}{0}_{M_{\psi_L^1}} \binom{0}{0}_{M_{\psi_L^2}}} C^{\overset{\psi_L}{Wx}}_{r-k,s-l} \acute{\mu}^{\overset{\psi_L}{Wx}}_{0,0} \\
&= C^{\overset{\psi_L}{Wx}}_{r-k,s-l} - C^{\overset{\psi_L}{Wx}}_{r-k,s-l} = 0.
\end{aligned} \tag{2.40}
$$

Having $J_{r-k,s-l} = 0$, the only term remaining in (2.39) is $C^{\overset{\psi_L}{Wy}}_{r,s}$. Therefore, $C^{\overset{\psi_L}{Wy}}_{r,s} = C^{\overset{\psi_L}{Wx}}_{r,s}$.

Theorem 4 is only valid when the blur operator is centrally symmetric and energy-preserving. In order to eliminate the energy-preserving restriction, a modification is necessary. A non-energy-preserving system $\tilde{b}$ could be represented as

$$\tilde{b} = m^{\tilde{b}}_{0,0} b, \tag{2.41}$$

where $b$ is an energy-preserving system. Therefore by introducing $\nu^y_{p,q} = \mu^y_{p,q}/\mu^y_{0,0}$ and equivalently $\acute{\nu}^y_{r,s} = \acute{\mu}^y_{p,q}/\acute{\mu}^y_{0,0}$, $m^{\tilde{b}}_{00}$ will be eliminated by becoming equal to one, and Theorem 4 could be modified accordingly.

**Theorem 5:** *For $\overset{\psi_L}{Wx}$, which is the wavelet transform of $x \in \mathbf{L^1}(\mathbb{Z}^2)$ with wavelet function $\psi_L \in \mathbf{L^2}(\mathbb{Z}^2)$, $D^{\overset{\psi_L}{Wx}}_{r,s}$ is invariant to centrally symmetric blur operators.*

$$
D^{\overset{\psi_L}{Wx}}_{r,s} = \begin{cases} \acute{\nu}^{\overset{\psi_L}{Wx}}_{r,s} - \underbrace{\sum_{i=0}^{r}\sum_{j=0}^{s}}_{0<i+j<r+s} \frac{\binom{r}{r-i}_{M_{\psi_L^1}} \binom{s}{s-j}_{M_{\psi_L^2}}}{\binom{i}{0}_{M_{\psi_L^1}} \binom{j}{0}_{M_{\psi_L^2}}} D^{\overset{\psi_L}{Wx}}_{r-i,s-j} \acute{\nu}^{\overset{\psi_L}{Wx}}_{i,j}, & (r+s)\ \textit{odd} \\ 0, & (r+s)\ \textit{even}. \end{cases}
\tag{2.42}
$$

Proof The proof is similar to that of Theorem 4.

**Corollary 2:** *The spatial domain blur invariants [17] are a special case of the proposed invariants in the wavelet domain.*

Proof Assume $h$ and $g$ are equal to 1. They are obviously not wavelet filters any more. Then, $\psi_1$ is found from (1.19), which is also 1, and it would have no vanishing moments ($M_{\psi_1^1} = M_{\psi_1^2} = 0$). The wavelet transform (eq. 1.18) of signal $x$ with this wavelet function is equivalent to itself ($\overset{\psi_L}{Wx} = x$). Also, $r + M_{\psi_L^1} = r + 0 = p$, $s + M_{\psi_L^2} = s + 0 = q$, $\mu_{p,q} = \acute{\mu}_{r,s}$, and $\binom{a}{b}_0 = \binom{a}{b}$. Replacing these

changes in (2.35) produces (2.43),

$$C^x_{p,q} = \begin{cases} \mu^x_{p,q} - \dfrac{1}{\mu^x_{0,0}} \underbrace{\sum_{i=0}^{p}\sum_{j=0}^{q}}_{0<i+j<p+q} \binom{p}{p-i}\binom{q}{q-j} C^x_{r-i,s-j}\mu^x_{i,j}, & (p+q)\ odd \\ 0, & (p+q)\ even \end{cases} \tag{2.43}$$

which is the blur invariant in the spatial domain.

## 2.7 Experiment 3

In this section, the performance of the proposed technique is evaluated on three different problems. The first experiment is designed to study how different types of blur affect the proposed invariants; three benchmark images are artificially degraded, and the changing of the value of the proposed blur invariants with different wavelet functions at different branches are studied. By branch, we mean all the possible combinations of wavelet and scaling filters at a certain level. For example, the branches when $L = 1$ are $g - g$, $g - h$, $h - g$, and $h - h$.

In the second experiment, a database of different objects are degraded with different blurs and noises in order to evaluate the performance of the invariants in a recognition task. In this experiment, the spatial domain invariants [17] are also employed for the sake of comparison.

In the third experiment, real-world degraded images are acquired, and the invariants are used for registration. The spatial domain blur invariants are used here as well for a comparison.

Three different wavelet functions are employed for these experiments: Coiflet of orders 1 and 2 [11], and Daubechies of order 3 [11]. These wavelet filters have 2, 4, and 6 vanishing moments, respectively.

### 2.7.1 Blur Effect

In the first experiment, three well-known benchmark photos are employed: Lena, Barbara (this photo is cropped in order to only include the face region), and Elaine, the sizes of which were 128×128. These photos are first degraded with circular averaging, energy preserving filters of different radii (5, 10, and 15). The original images and the degraded ones are represented in Figure 2.5. The blur invariants (eq. 2.35) of all these images were calculated with Coiflet of order 1 at three different levels. The calculated moments are of 9 different orders, and they are represented in Table 2.3. For the sake of clarity, the order of magnitudes of moments are shown beside the order of the moments in the table. Furthermore, the same experiment is repeated after degrading these photos

with Gaussian blur of size 10, 20, and 30 with standard deviation 2, 5, and 7 respectively. Nine of the blur invariants of these images are calculated with Coiflet of order 2 at three different levels, which are represented in Table 2.4. As the tables read, the different subjects of the photos are distinguishable from each other using the moments, and the blur intensity increase does not affect the blur invariant descriptors. The small observed changes in their values are particularly because the signals are finite-extended. Candocia discusses this issue [7], and points out the specific criteria that are required to have similar features perfectly invariant when the signal is finite-extended.

The photos are also degraded by motion filters which are not energy-preserving (Figure 2.6). The first filter represents a horizontal motion of length 20 and decreases the image energy by half. More specifically, the zero order moment of the filter is 0.5 ($m^b_{00} = 0.5$). The second filter describes a vertical motion of the same length and increases the image energy by half ($m^b_{00} = 1.5$). Since the maximum value of each pixel is 255, saturation happens if the intensity is greater than 170. It means that a homogeneous increase of energy is not possible in this case, which introduces a non-uniform change of intensity.

Since the filters are not energy-preserving any more, the blur invariants in Eq. (2.42) are utilized. The employed wavelet function was Daubechies of order 3. The value of 9 different moments are represented in Table 2.5. It shows that the change in the values of moments is very negligible once the images are degraded with the first filter. The change becomes a little more considerable in degraded images with the second filter and in moments of higher orders and further branches, specifically in Elaine's image. However, it is still possible to perfectly distinguish between different images using their blur invariants.

### 2.7.2 Noise Effect

In the second experiment, the blur invariants are employed in a simple pattern recognition application. In this experiment, ten images (Figure 2.7) from the COIL-100 database [52] are chosen. These images are blurred with disk, Gaussian (with its $\sigma$ equal to one fifth of the size of the mask), and motion (at angles 0, 30, 60, and 90) blurs with mask of sizes of 5×5, 9×9, 13×13, 17×17, and 21×21. These 300 blurred photos form the test set of the experiment, and are contaminated with Gaussian and salt and pepper noises. Then, their blur invariants are calculated, compared to those of the original images, and are classified based on the distance between them. The wavelet based moment invariants of orders up to 13 ($r + s = 13$) are calculated with Daubechies of order 3 at four different branches: 1) $hhg - hhg$, 2) $ghh - ghh$, 3) $hhhg - hhhg$, and 4) $ghhg - ghhg$. In order to make a comparison, the blur invariants proposed in [17] is also used in this experiment.

Table 2.3: blur invariants of degraded images with disk filters. Coiflet of order 1 is employed for this experiment.

| Branch | | $g-h$ | | | $hg-gg$ | | | $ghg-hhg$ | | |
|---|---|---|---|---|---|---|---|---|---|---|
| (r,s)/O.M. | | (0,5)/12 | (3,6)/22 | (6,9)/38 | (0,3)/10 | (5,2)/20 | (7,4)/30 | (4,1)/36 | (2,7)/26 | (8,5)/16 |
| Image | Blur | | | | | | | | | |
| Lena | 0 | -52.34 | -6.98 | 1.71 | 46.03 | 3.65 | 7.85 | -2.77 | -2.82 | -4.21 |
| | 5 | -52.39 | -6.94 | 1.70 | 46.08 | 3.62 | 7.78 | -2.74 | -2.79 | -4.19 |
| | 10 | -52.71 | -6.80 | 1.66 | 46.43 | 3.47 | 7.49 | -2.60 | -2.64 | -4.09 |
| | 15 | -53.23 | -6.54 | 1.60 | 47.02 | 3.18 | 6.95 | -2.32 | -2.33 | -3.93 |
| Barbara | 0 | 4.38 | -13.58 | 2.58 | -3.09 | 14.65 | 25.80 | -7.35 | -16.69 | -6.21 |
| | 5 | 4.47 | -13.55 | 2.57 | -3.17 | 14.64 | 25.64 | -7.28 | -16.64 | -6.18 |
| | 10 | 4.35 | -13.31 | 2.51 | -3.07 | 14.45 | 25.04 | -7.09 | -16.36 | -6.02 |
| | 15 | 4.10 | -12.97 | 2.42 | -2.88 | 14.16 | 24.23 | -6.86 | -15.96 | -5.81 |
| Elaine | 0 | 50.13 | -16.25 | 5.79 | -34.15 | 9.84 | 25.46 | -6.58 | -10.57 | -12.47 |
| | 5 | 49.89 | -16.19 | 5.76 | -33.98 | 9.81 | 25.35 | -6.56 | -10.55 | -12.41 |
| | 10 | 49.26 | -16.07 | 5.71 | -33.58 | 9.78 | 25.15 | -6.52 | -10.50 | -12.30 |
| | 15 | 48.36 | -15.91 | 5.63 | -33.01 | 9.71 | 24.85 | -6.47 | -10.42 | -12.15 |

Table 2.4: blur invariants of degraded images with Gaussian filters. Coiflet of order 2 is employed for this experiment.

| Branch | | $h-g$ | | | $hg-gh$ | | | $ghh-hhg$ | | |
|---|---|---|---|---|---|---|---|---|---|---|
| (r,s)/O.M. | | (6,1)/16 | (3,8)/30 | (10,5)/39 | (1,2)/12 | (8,1)/26 | (9,8)/49 | (0,5)/17 | (6,5)/33 | (9,4)/38 |
| Image | Blur | | | | | | | | | |
| Lena | 0 | -9.54 | -3.83 | -7.60 | -6.09 | -4.36 | -3.83 | -20.06 | 3.12 | -7.26 |
| | 10,2 | -9.31 | -3.63 | -7.33 | -6.46 | -2.27 | -3.71 | -19.90 | 3.04 | -6.87 |
| | 20,5 | -8.49 | -3.58 | -7.07 | -6.25 | 3.08 | -3.61 | -20.00 | 2.96 | -6.59 |
| | 30,7 | -7.31 | -3.51 | -6.71 | -5.94 | 10.65 | -3.47 | -20.14 | 2.87 | -6.19 |
| Barbara | 0 | -70.08 | -5.79 | -31.13 | 16.38 | -680.09 | -8.57 | 1.68 | 6.24 | -32.84 |
| | 10,2 | -68.32 | -5.79 | -31.17 | 16.39 | -665.85 | -8.65 | 1.43 | 6.23 | -32.68 |
| | 20,5 | -66.97 | -5.71 | -30.55 | 16.49 | -653.68 | -8.43 | 1.41 | 6.14 | -32.00 |
| | 30,7 | -65.54 | -5.60 | -29.78 | 16.49 | -640.56 | -8.15 | 1.35 | 6.03 | -31.24 |
| Elaine | 0 | -51.81 | -9.24 | -32.71 | 6.66 | -406.91 | -17.36 | 19.21 | 7.77 | -30.23 |
| | 10,2 | -51.64 | -8.86 | -32.43 | 6.54 | -406.66 | -17.11 | 20.04 | 7.63 | -29.96 |
| | 20,5 | -51.31 | -8.80 | -32.16 | 6.60 | -404.49 | -16.94 | 19.82 | 7.58 | -29.72 |
| | 30,7 | -51.01 | -8.74 | -31.86 | 6.66 | -402.41 | -16.74 | 19.57 | 7.51 | -29.45 |

Table 2.5: blur invariants of degraded images with motion, non-energy-preserving filters. Daubechies of order 3 is employed for this experiment.

| Branch | | $g-g$ | | | $gg-gh$ | | | $hgh-hgg$ | | |
|---|---|---|---|---|---|---|---|---|---|---|
| (r,s)/O.M. | | (2,3)/10 | (9,0)/21 | (7,10)/41 | (4,3)/15 | (2,9)/26 | (6,7)/31 | (1,2)/5 | (10,1)/25 | (7,8)/37 |
| Image | Blur | | | | | | | | | |
| Lena | 0 | -3.11 | 3.16 | -6.32 | 13.27 | 2.68 | -7.99 | -11.50 | -8.17 | 3.15 |
| | 20-0-0.5 | -3.04 | 3.14 | -6.16 | 12.82 | 2.67 | -7.78 | -10.87 | -9.51 | 2.99 |
| | 20-90-1.5 | -2.45 | 2.83 | -4.86 | 10.64 | 2.14 | -6.23 | -10.44 | -7.86 | 2.49 |
| Barbara | 0 | -2.22 | -5.95 | -9.72 | 19.84 | 2.90 | -16.88 | 32.27 | 138.32 | 5.24 |
| | 20-0-0.5 | -2.20 | -5.91 | -9.48 | 18.46 | 2.75 | -14.87 | 34.23 | 148.12 | 6.78 |
| | 20-90-1.5 | -2.22 | -5.38 | -8.39 | 17.54 | 2.50 | -13.24 | 31.28 | 141.17 | 6.10 |
| Elaine | 0 | -2.54 | -1.77 | -23.91 | 17.39 | 4.22 | -21.31 | 11.20 | 57.64 | 10.10 |
| | 20-0-0.5 | -2.50 | -1.77 | -23.69 | 17.24 | 4.18 | -21.16 | 11.57 | 59.97 | 10.63 |
| | 20-90-1.5 | -1.13 | -1.77 | -11.12 | 9.31 | 1.88 | -11.27 | 9.89 | 40.78 | 5.29 |


Figure 2.5: Images of Lena, Barbara, and Elaine in their original shape and blurred with disk filters of different radii.

Figure 2.8 shows the average classification rate of 20 tests in the presence of Gaussian noise. The standard deviation of the noise changes from 0 (without noise) to 25. When there is no noise, the achieved accuracy rate with different invariants are perfect, which shows that the change of blur intensity does not affect the classification rate at all. This, however, changes when noise is introduced to the images. Invariants of different branches respond differently to the introduction of noise. The invariants that are calculated at branches $hhg - hhg$ and $hhhg - hhhg$ show higher robustness to noise than the spatial domain blur invariants. On the other hand, the invariants that are calculated at branches $ghhg - ghhg$ and $ghh - ghh$ have poor performances comparing to the spatial domain blur invariants.

The test is also repeated with salt and pepper noise. In this case, the density of noise is increased from 0 (no noise) to 5%, which means that 5% of the number of pixels are contaminated with this noise. The average classification rate of twenty tests in the presence of this noise is presented in Figure 2.9. Similar to the previous test, the calculated invariants at branches $hhg - hhg$ and $hhhg - hhhg$ outperformed the spatial domain invariants, while the invariants from branches $ghhg - ghhg$ and


Figure 2.6: Images of Lena, Barbara, and Elaine in their original shape and blurred with motion filters of different directions and energies.


Figure 2.7: Ten images from COIL100 database that are used in the second experiment.

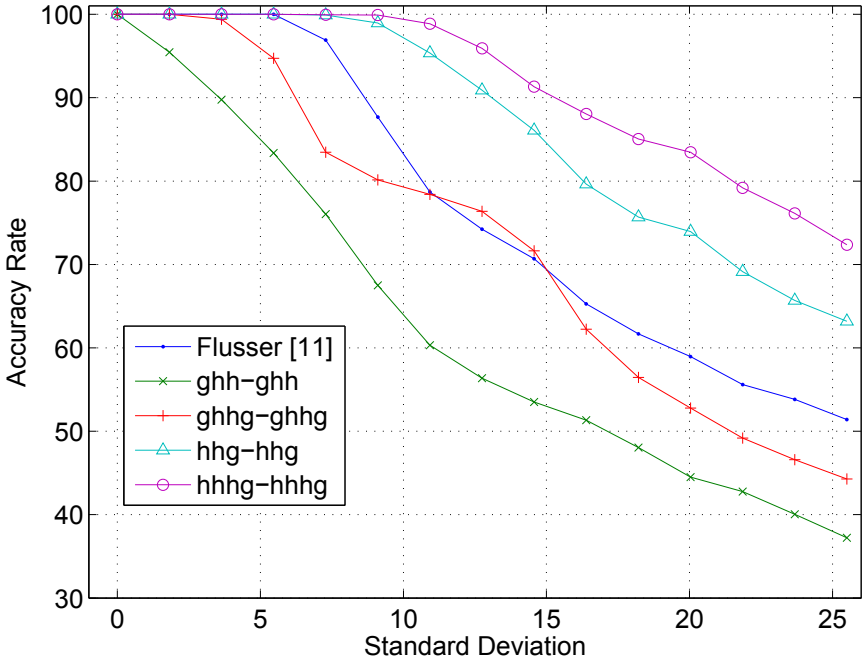


Figure 2.8: Accuracy rate in the presence of Gaussian noise.

$ghh - ghh$ show less robustness.

The reason behind a rapid drop in the performances of the calculated invariants at branches $ghh-ghh$ and $ghhg - ghhg$ is that they filter most of the low frequency band, keeping the high frequencies which are more sensitive to noise. Therefore, their accuracy rates drop significantly by the increase of the noise intensity. $hhg-hhg$ and $hhhg-hhhg$, on the other hand, filter the high frequency band, thus show a better robustness to the noise increase. Figure 2.10 shows the magnitude response of these filters in one dimension.

### 2.7.3 Registration

In this experiment, the invariants are used in a registration task. One sharp and three out of focus photos are taken of an outdoor scene, and a part of the sharp image is chosen as the template for registration in other degraded images. Figure 2.11 shows the source image, where the template is illustrated in a window. The out of focus images are presented in Figure 2.12. From left to right, the camera was focused at 50, 10, and 1 meter(s), respectively. The size of the images is 212×282 and the template is 43×48. For this experiment, Coiflet of order 1 is exploited as the wavelet function, and moments of orders up to 10 ($r + s = 10$) are calculated at branch $hh - hh$. For the sake of

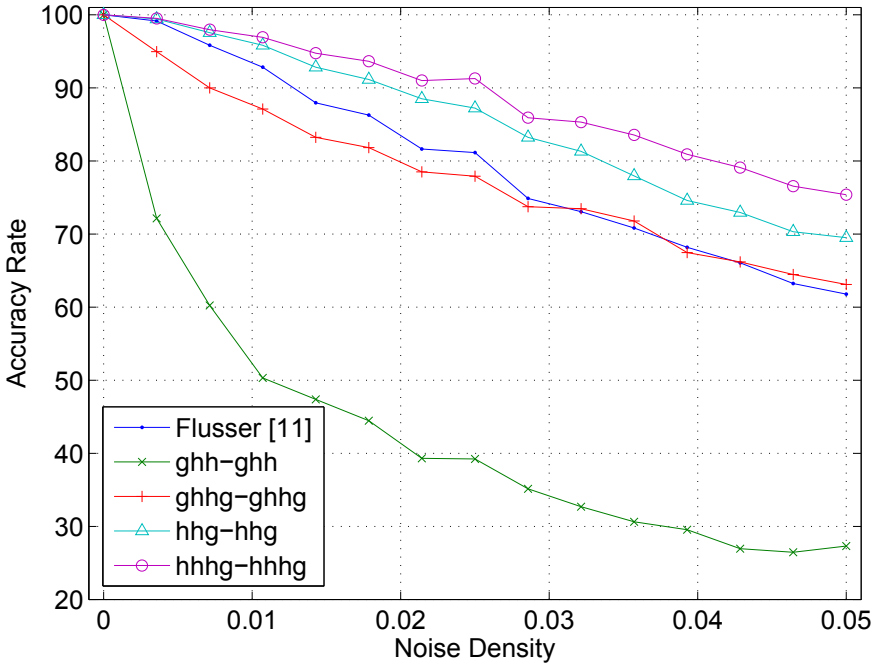


Figure 2.9: Accuracy rate in the presence of salt and pepper noise.

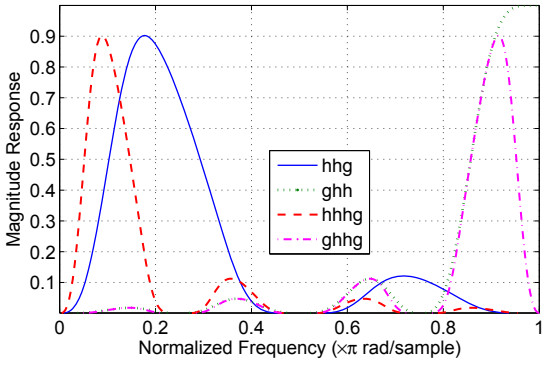


Figure 2.10: The magnitude responses of the filters used in the second experiment.

Figure 2.11: The source image in registration. The template is illustrated with a window.

comparison, spatial domain blur invariants of orders up to 10 are also used. For registration, a window of the same size of the selected template is chosen, and the corresponding moments of that section of the image are calculated. This window is moved all around the image until it scans it thoroughly. Afterwards, the following measure is used to calculate the similarity of the template to every subsection of the image.

$$S_{ij} = \exp\left(-\sum_{n=1}^{N}\left|\frac{B^{y_{ij}}(n) - B^{x}(n)}{B^{x}(n)}\right|\right) \tag{2.44}$$

In (2.44), $B$ is the array of calculated invariants, $N = 16$, $x$ is the template, and $y_{ij}$ is a subsection of the target photo with its centre at $(i, j)$.

Figure 2.11 also shows where the template is registered using the wavelet and spatial domain blur invariants. The registration with the wavelet domain blur invariants is accurate, while using the spatial domain blur invariants, the exact location in one of the images is missed.

## 2.8 Discriminative Power

Flusser and Suk [17] showed that if signals are centrally symmetric, their blur invariants are equal to zero, which means that it is impossible to distinguish between different centrally symmetric signals. The same statement is true regarding the proposed invariants in a case where the signal and the wavelet function are both centrally symmetric. In this case, $m_{p,q}^{\overset{\psi}{W}_{L}^{x}}$ is zero when $p + q$ is odd, which can be easily inferred from (2.30). The odd order moments of a signal in the wavelet

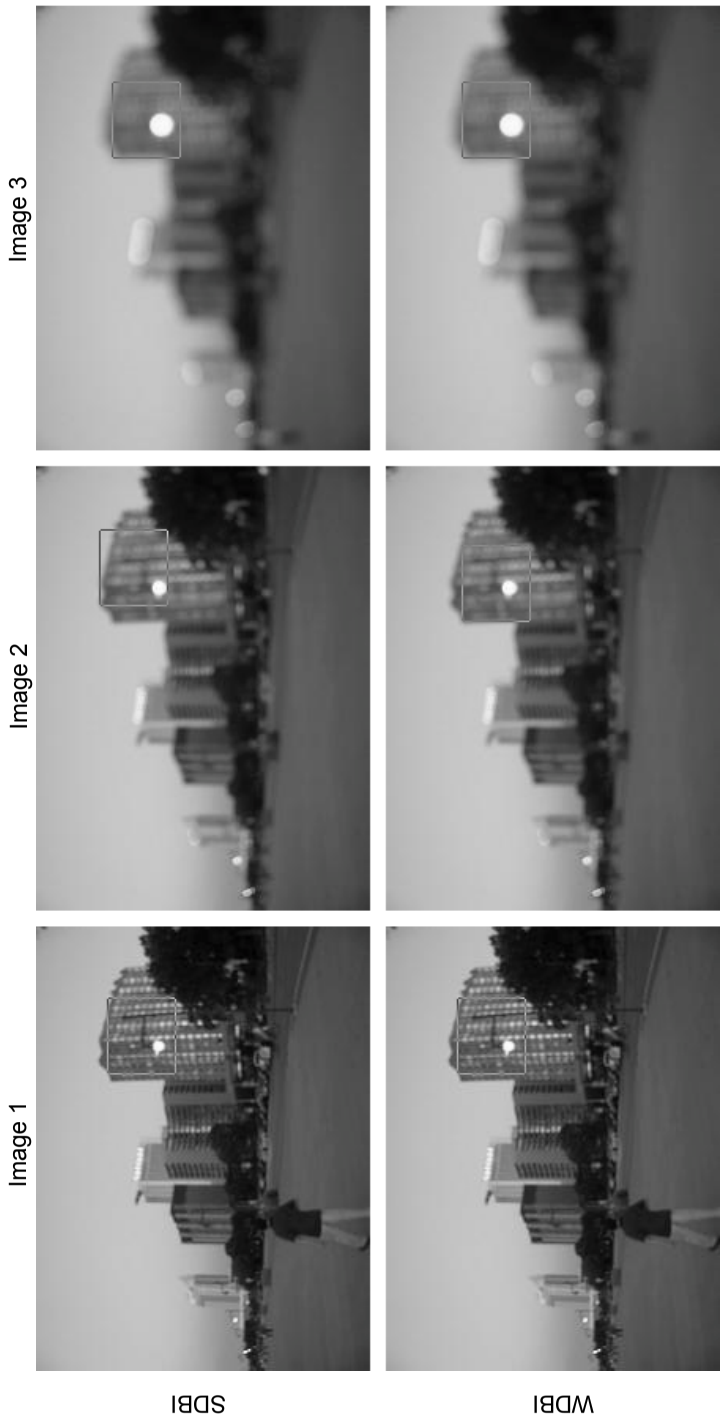


Figure 2.12: The registration results with spatial domain blur invariants (SDBI) and wavelet domain blur invariants (WDBI). Using SDBIs, one of the images is not registered correctly, while using WDBIs did not cause any problem.

domain is the summation of odd order moments of the signal in the spatial domain multiplied by even order moments of the wavelet function and even order moments of the signal in the spatial domain multiplied by odd order moments of the wavelet function. This also puts $\mu_{p,q}^{\psi_L^{W_x}}$ equal to zero, and since the odd order central moments are zero, $C_{r,s}^{\psi_L^{W_x}}$ becomes zero as well. However, if the selected wavelet function is not centrally symmetric, $m_{p,q}^{\psi_L^{W_x}}$ and subsequently $\mu_{p,q}^{\psi_L^{W_x}}$ would not be zero. The reason is that the odd order moments of the wavelet function in (2.30) are not zero any more, which proves that $C_{r,s}^{\psi_L^{W_x}}$ is nonzero as well. Therefore, the limitedness of discriminative power which is addressed by Flusser and Suk [17] is not an issue in the wavelet domain blur invariants.

However, there are three cases that can produce null spaces for the proposed invariants, which are avoidable by a choice of wavelet function. First, the wavelet transform of a polynomial of order $N$ with a wavelet function with $M$ vanishing moments is zero, where $M>N$, and therefore it will be impossible to distinguish between different polynomials of such orders. Second, the invariants of images that their wavelet transform with a non-symmetric wavelet function become symmetric will be equal to zero. Third, if two images differ one another by a polynomial term of order $N$, and a wavelet function with $M$ vanishing moments is employed, where $M>N$, then the proposed invariants would not be able to discriminate them. It is always possible to avoid such null spaces by employing an alternative wavelet function. The realization of the third case could be a gradual change of illumination in images, and mostly it is desirable the descriptors to be invariant to such changes. It is worth mentioning that the occurrence of such cases are fairly rare.

## 2.9 Conclusion

In this chapter, a new set of blur invariant descriptors is proposed. These descriptors are developed in the wavelet domain for 1D continuous and 1D and 2D discrete signals to be invariant to centrally symmetric blur. Defining them in the wavelet domain grants them the advantages that this domain has, i.e. different alternatives of bases, and analysis at different scales. The spatial domain blur invariants are also proved to be a special case of these invariants. In a discussion on the discriminative power of the proposed blur invariants, it is shown how they would not have null space for centrally symmetric signals, which is the problem that the conventional invariants have, and although the chance of occurrence is low, it subsequently reduces their discriminative power.

In order to evaluate the performance of these invariants, different experiments have been carried out. In the first experiment with artificial 1D signals in section 2.3, it is shown that the wavelet domain blur invariants do not vary by the change of blur intensity. On the other hand, noise intensity can

change their values to some extent. This is while the spatial domain blur invariants showed to be more susceptible to noise. In another experiment on noise effect, which came in section 2.7.2, cases of which the proposed blur invariants could perform not as good as the spatial domain blur invariants are also studied. It all comes down to the choice of branches for wavelet decomposition, which could either make these invariants perform better or worse that the conventional ones. This is expectable since some subbands in wavelet transform are more sensitive to noise than others.

In another experiment with EEG signals in section 2.5, the invariants performed well discriminating properly between different signals and showing very little variation due to changes in blur system effect. In a similar experiment (section 2.7.1), three well-known images were employed and artificially degraded with different blurring filters. The invariants successfully could put a discrepancy between different subjects, while showing very negligible difference due to the degradations introduced by blur.

In the third experiment, there were photos taken such that the scenes were deteriorated by defocus blur. Then, a part of the scene, which was selected from a sharp photo, was used as templates for image registration. Despite the presence of severe blurs, registration was performed perfectly. The experiment was carried out with the spatial domain blur invariants which failed in one of the registration tasks.

# Chapter 3

# *Face Recognition with Blurred Faces*

## 3.1 Introduction

There has been a growing interest and research in face recognition. However, many of the proposed systems work with only images taken under perfect conditions. There are still challenges that should be tackled in order to have a system that works in unconstraint environments [38]. Different involved factors in a such an environment could make having a nearly acceptable face image impossible, let alone perfect: poor lightning condition introduces illumination to the image, a non-cooperative subject brings on challenges such as wide pose variations and severe occlusions, and a moving subject, an on-focused camera, or a long distance between the camera and the subject introduce different sorts of blurs to the image. The problems related to illumination, pose, and occlusion are hot topics in face recognition research. However, blur has been relatively overlooked for some unknown reasons.

Blur affects faces in images in two different ways [54]: (1) the appearance of faces changes due to blur, and (2) face images of different people tend to look similar. To alleviate this problem, there are different types of approaches developed. One of the early stage methods for dealing with blur was removing it. This is basically a deconvolution problem aiming at finding the parameters of the blur system in order to perform the deconvolution [63, 8]. Xin et. al [75] came up with an statistical model for debluring face images. In their approach, the problem of debluring is changed into an optimization problem on their proposed model. A series of approaches adopt more than

one image in order to reconstruct a sharp image. In Wheeler's algorithm [73], Active Appearance Model (AAM) was employed along with Wiener filter to acquire a sharp face image from a video sequence. In order to avoid computational expenses, deblurring was later proposed to be shifted to the feature extraction step: Gunturk and Batur [23] proposed a super-resolution method in the eigneface domain which is applicable on videos.

Producing overcomplete database is another approach that has become popular in tackling blur. In this approach, a database with sharp images is artificially degraded with different blur filters. Stainvas and Intrator [68] proposed a hybrid neural network for recognition and restoration of blurred images. The training of the network was performed by artificially blurred images. Fiche et. al. [13] employed a blur metric for measuring the blur intensity in the query image. Having that, a proper set of images from their overcomplete database is used, which have the nearest blur intensity. Nishiyama et. al. [54] proposed a classification based on the blur intensity of the query image, prior to face recognition. Using an overcomplete database, the statistical models of blur appearance is learnt. Based on them, the blur model of the query image is inferred, and using the corresponding blur model, the image is deblurred.

In all of the described techniques, identification of the blur system is involved at some level before using it for recognition. An alternative approach is to extract features that are invariant to blur. The blur invariant techniques have been comprehensively surveyed in the last chapter. However, except one of them, they have not been used in face recognition problems yet. Local Phase Quantization (LPQ) which had been initially proposed by Ojansivu and Heikillä [58] for texture classification, was employed by Ahonen et. al. [1] to produce LPQ face descriptors.

In this chapter, the blur invariants that were developed in chapter 2 are used for face recognition. Also by introducing an alternative definition for moments, blur invariants are redefined based on them. In the next section, the general architecture of the face recognition system that is used in this chapter is explained. Section 3.3 studies the performance of the blur invariants from chapter 2. An alternative definition for ordinary moments are proposed in section 3.4. Moreover, they are used in the same section to redefine the blur invariants in the spatial domain. Two schemes are proposed in section 3.5 which use the blur invariants of section 3.4 to produce a single feature vector. Sections 3.6 and 3.7 use the proposed schemes. Blur effect is studied on them, and their performances are compared with a similar technique as well. Section 3.8 concludes the chapter.

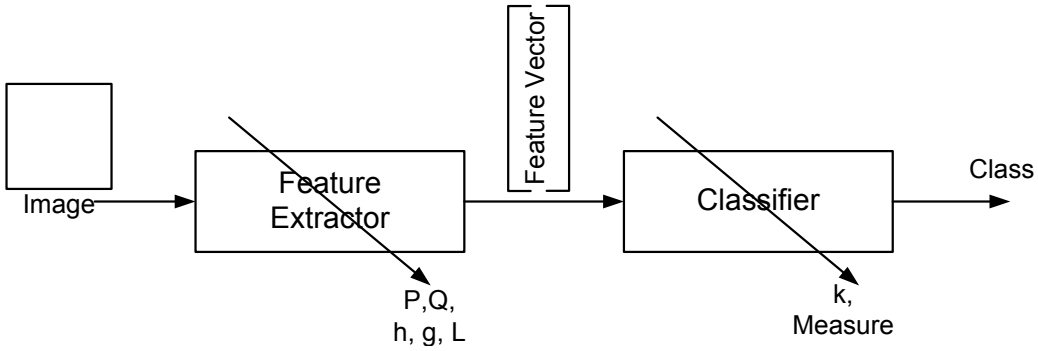


Figure 3.1: The face recognition architecture that is used in this thesis

## 3.2 Face Recognition System

The face recognition system that is used in this work is depicted in Figure 3.1. The system consists of the two essential units of a pattern recognition system: a feature extractor and a classifier. In the feature extraction unit, the blur invariants that were developed in chapter 2 or those that are proposed in this chapter are used. The required parameters are $P$ and $Q$, which define the order of the moments, $h$ and $g$, which are the wavelet filters, and $L$, the branch at which the blur invariants should be calculated.

Since the focus of this thesis is on feature extraction, a simple classifier is used to make a fair comparison possible. The classifier that is employed in this work is a $k$-nn with $k = 1$. The measure for calculating distance is Modified Sum of Squared Error (MSSE). It should be mentioned that no preprocessing method is used prior to feature extraction.

## 3.3 Experiment 1: Face Recognition with Blur Invariant on AT&T Database

For face recognition with blur invariants, both the spatial domain and wavelet domain blur invariants were used. The preliminary test was carried out on the AT&T (Figure 3.2) database. This database includes 400 different images of 40 individuals, 10 of each. In the experiments of this chapter, these images were resized to be 128×128. In order to study the blur effect on the accuracy rate, 5 out of 10 images per person were randomly chosen as the gallery set, and the rest were artificially blurred with Gaussian filters with different standard deviations to model different intensities of defocus

Figure 3.2: Samples from the AT&T database

blur. The standard deviation of the filters were changed from 0.2 to 5.8. Figure 3.3 shows how these filters affect a face image. The blur invariants of orders up to 35 were calculated. For the wavelet domain blur invariants, Coiflet or order 1 (COIF1) was used to calculate the invariants at $hh - hh$, $hhg - hhg$, and $hhhg - hhhg$ branches. The employed classifier was $k$-nn with $k = 1$ and Modified Sum of Squared Error (MSSE). For a comparison with a benchmark method, eignenface technique [72] was employed as well.

Figure 3.4 shows the average of twenty trials. The blur invariants do not show a satisfactory performance; their accuracy rates stand very low, and decrease with the increase of blur intensity. What proves them to be unsuitable features for face recognition is when they are compared with eigenface, a benchmark feature extraction technique for face recognition. This method shows a better performance, and although it drops really fast by the increase of blur, it is only for the standard deviation of 5.8 that it stands lower than the blur invariants. The change of the number of involved blur invariants in classification does not affect the recognition rate significantly unless it is as low as 4, where the classification rate drops drastically. Therefore, the chance of having a good classification rate by having a proper number of invariants is almost zero.

## 3.4 Blur Invariant Descriptors

There is a problem with using geometric (ordinary or central) moment based blur invariants in face recognition applications: the bases, $\{x^p | p \in \mathbb{N}^0\}$, that are used in these moments are not orthogonal, producing redundant information [76]. An analytical discussion on information redundancy

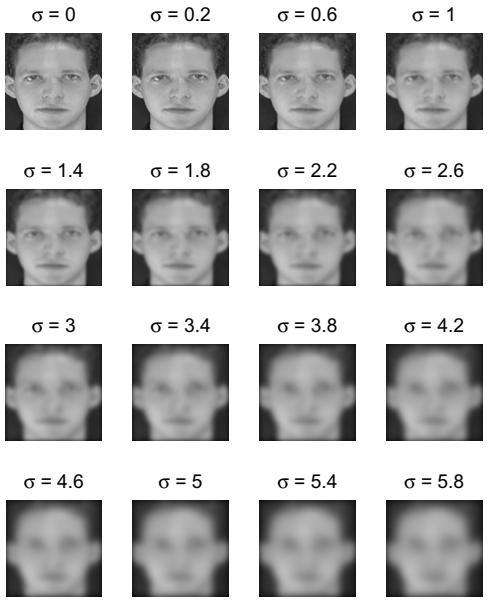


Figure 3.3: A face image from the AT&T database blurred with Gaussian filters of different sizes. $\sigma = 0$ is the case for the sharp image.

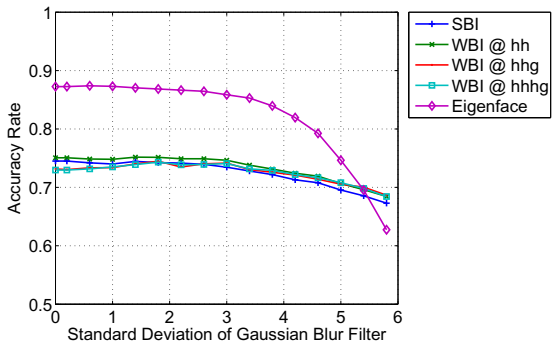


Figure 3.4: Classification accuracy rate on the AT&T database when artificially blurred with Gaussian filters. The spatial and wavelet domain blur invariants neither show a good discriminative power, nor they are invariant to blur effect. Eigenface approach shows a better classification rate comparing to the blur invariants, however, as it is expected, is less tolerable to blur.

of different types of moments [71] and satisfactory results [24, 51], that have been reported with orthogonal moments, are proofs of this statement. Also because of the bases' property, as the image size increases, the moments tend to put more weight on further pixels from the centroid, which means loss of information. Considering all of these in a face recognition problem, it is clear that using the blur invariants as they are cannot be very promising.

Since the employed blur invariants are based on ordinary moments, it is desirable to find a way to increase their discriminative power, rather than abounding them to adopt a different set of moments and invariants. In this section, with an alternative definition for ordinary moments, which makes a local concentration on pixels possible, the addressed problem is resolved. Also, it is shown that the blur invariants can be redefined based on them to increase their discriminative power.

**Definition 3.** *Assuming signal $x$ is $N_1 \times N_2$, and introducing $a[n,p]=(-n)^p$ with size $M_1 \times M_2$, the generalized ordinary moment (GOM) of $x$ is defined as*

$$Kx_{p,q}^{M_1\times M_2}[n_3,n_4] = \sum_{n_1=-t_1}^{t_1}\sum_{n_2=-t_2}^{t_2} a[n_1,p]a[n_2,q]x[n_3-n_1,n_4-n_2], \tag{3.1}$$

*where $t_i = \frac{M_i}{2}$ with $i = 1, 2$.*

The ordinary moments in (1.29) are a special case of (3.1); if $M_1 = N_1$ and $M_2 = N_2$, then $Kx_{p,q}^{M_1\times M_2}[0,0] = m_{p,q}^x$.

As $M_1$ and $M_2$ become smaller, GOMs would contain relatively more local information of the image. The effect of $M_i$ is studied later in this section.

An advantage that GOMs have over the ordinary moments is that if an image is shifted, its GOMs will be shifted for the certain amount and in the same direction, without changing its value. In another word, while shift translates into change of values in ordinary moments, it simply keeps its nature in GOMs.

Flusser's blur invariants in the spatial domain, which are developed based on central moments, can be utilized with GOMs in order to have blur invariant descriptors (BID). The following theorem, which is derived from (2.43), represents BIDs that are based on GOMs.

**Theorem 6:** *For $x \in \mathbf{L^1}(\mathbb{Z}^2)$, $BIDx_{p,q}^{M_1\times M_2}$ is invariant to energy-preserving, centrally symmetric blur operators.*

$$BIDx_{p,q}^{M_1\times M_2} = \begin{cases} Kx_{p,q}^{M_1\times M_2} - \dfrac{1}{Kx_{0,0}^{M_1\times M_2}} \underbrace{\sum_{i=0}^{p}\sum_{j=0}^{q}}_{0<i+j<p+q} \binom{p}{p-i}\binom{q}{q-j} BIDx_{p-i,q-j}^{M_1\times M_2} Kx_{i,j}^{M_1\times M_2}, & (p+q)\,odd \\ 0, & (p+q)\,even \end{cases} \tag{3.2}$$

Proof The proof is similar to that of Theorem 4 and Corollary 2.

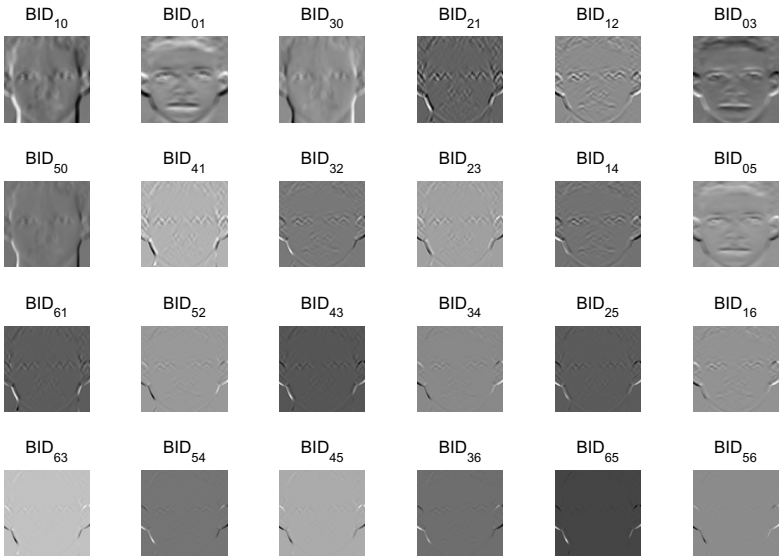


Figure 3.5: BIDs of a face image obtained with a 8×8 window. They are rescaled for representation.

$BID_{p,q}^{8\times8}$ of the original face image in Figure 3.3 are shown in Figure 3.5 as an example.

It is expected that the BIDs of a blurred image to be similar to those of the original image, showing no sensitivity to the blur intensity. However, $M_1$ and $M_2$ affect the BIDs' tolerance to blur. Figures 3.6 show the $BID_{p,q}^{8\times8}$s and $BID_{p,q}^{64\times64}$s of the images in Figure 3.3. The effect of blur becomes obvious in Figure 3.6a as soon as $\sigma$ reaches 1. This is while the BIDs in Figure 3.6b demonstrate a very high tolerance to blur, and the descriptors stay almost the same for all $\sigma$s. Figure 3.7 shows the effect of $M$ versus $\sigma$. The $z$-axis is the distance between the $BID_{05}^{M\times M}$ of the original image in Figure 3.3 and those of the blurred images in the same figure, where $M = 8:4:64$. The distance is calculated with

$$d = \sum_{n_1}\sum_{n_2}\left|\frac{BIDx_{p,q}^{M_1\times M_2}[n_1,n_2] - BIDy_{p,q}^{M_1\times M_2}[n_1,n_2]}{BIDx_{p,q}^{M_1\times M_2}[n_1,n_2]}\right|, \tag{3.3}$$

where $x$ and $y$ are the original and blurred signals, respectively, $p$ is 0, and $q$ is equal to 5. As the figure shows, the BID of smaller window sizes are more sensitive to blur intensity variation. The reason is that by the increase of blur intensity (which means a larger blur operator matrix), the number of neighbouring pixels in forming a pixel in the degraded image grows. In this case, if the chosen window for calculating the GOMs, and consequently the BIDs, does not cover all of these pixels, then the BIDs would not be relevant, which consequences in a set of poor BIDs. On the other hand, if the window is large enough to include those pixels as well, the BIDs will show a reasonable

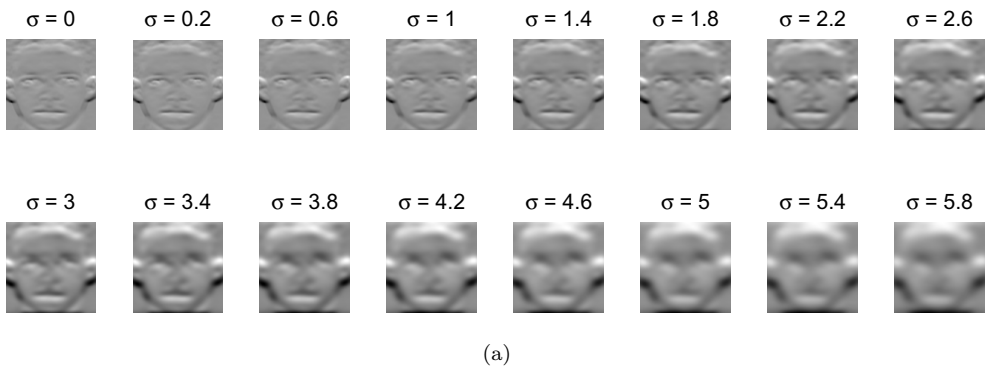


(a)

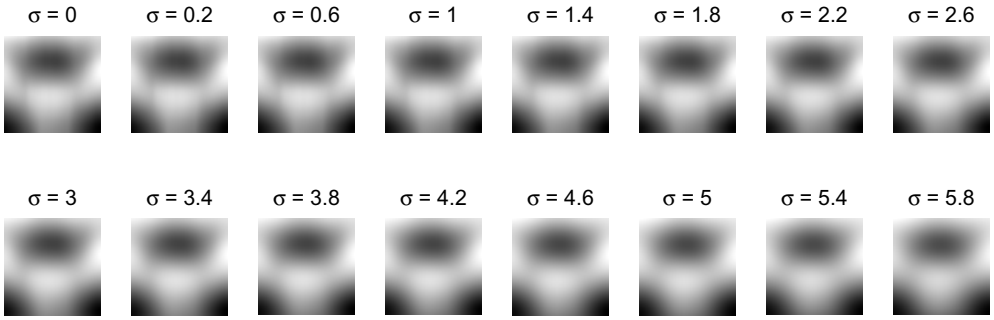


(b)

Figure 3.6: $BID_{05}$ of the images in Figure 3.3 obtained with (a) a 8×8 window (b) a 64×64 window. They are rescaled for representation.

robustness to that level of blur. This is the case for the BIDs that are calculated with windows of larger than 32×32 in this example. Having a large window might simply secure a face recognition system from a wide range of blur changes, however a larger window translates into losing more local information up to a point were the window is as big as the image, and the BIDs simply become the blur invariants that have been shown to have a very limited discriminative power for a large-scale patter recognition problem. This issue is addressed in the first part of 3.6.

## 3.5 Feature Extraction Schemes for Face Recognition

Two different schemes are proposed in this section for feature extraction. With these techniques, a single feature vector will be extracted from a set of BIDs.

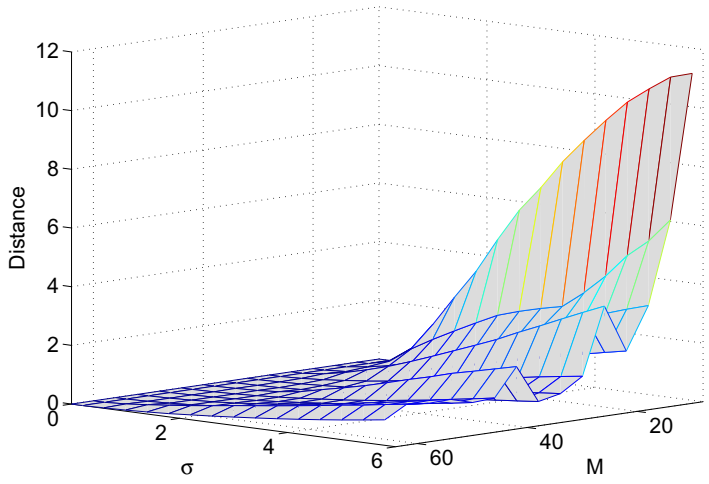


Figure 3.7: The distance between $BID_{05}^{M\times M}$ of a face image and those of the blurred ones where $M = 8 : 4 : 64$.

### 3.5.1 Eigenmoment Scheme

In this approach, similar to the technique of using eigenfaces [72], as they are called here, eigenmoments (EM) are calculated for each BID. Figure 3.8 shows the structure of the EM scheme. Having a gallery set, the BIDs of up to a certain order are calculated. Then, the EMs for each order are calculated and stored. Using these EMs, the weights of the BIDs of query image are calculated and concatenated after normalization. The produced vector will be used for classification.

### 3.5.2 Local Histogram Scheme

In this approach, which is presented in Figure 3.9, each BID is divided into a certain number of non-overlapping regions. By defining a number of bins, the histogram of each region is obtained. These histograms are concatenated in order to form a vector. The obtained vectors from different BIDs are put together to build a matrix. Finally, PCA is applied on this matrix for dimension reduction. The final feature vector can be used for classification.

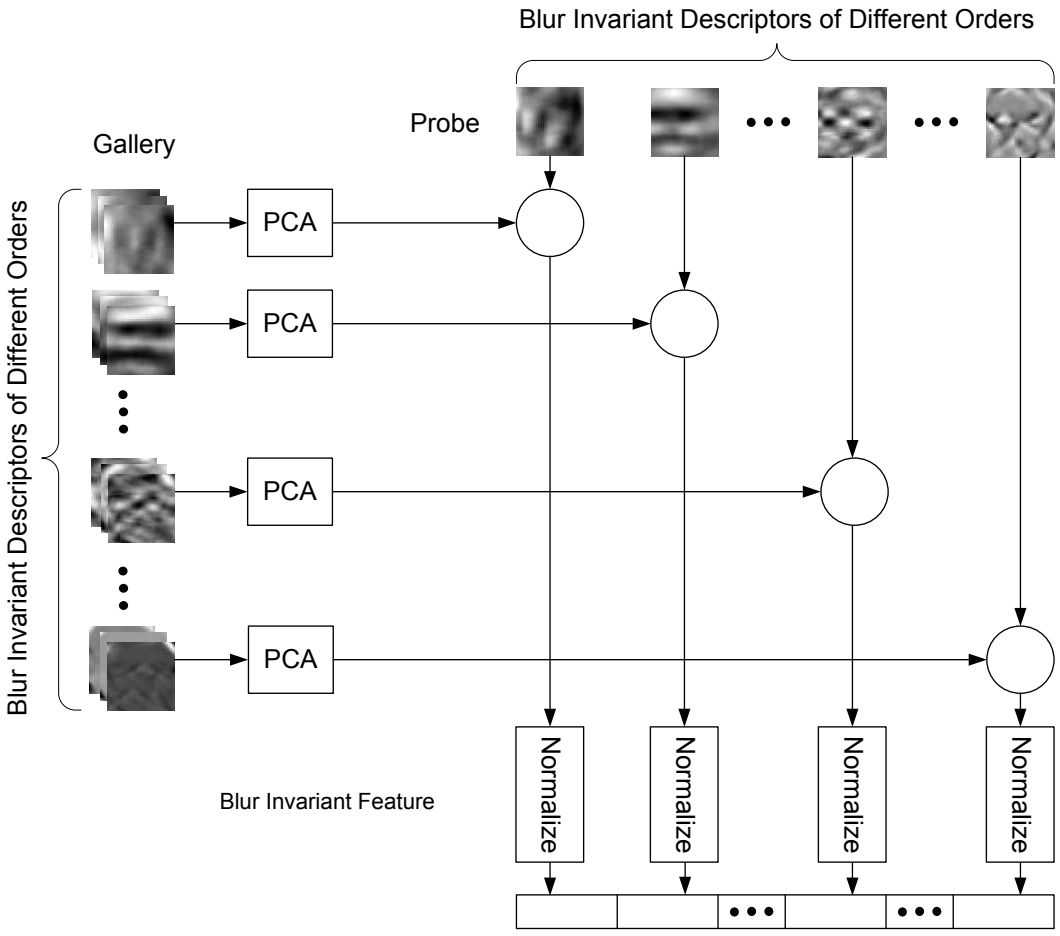


Figure 3.8: The Scheme for Eigenmoment Approach

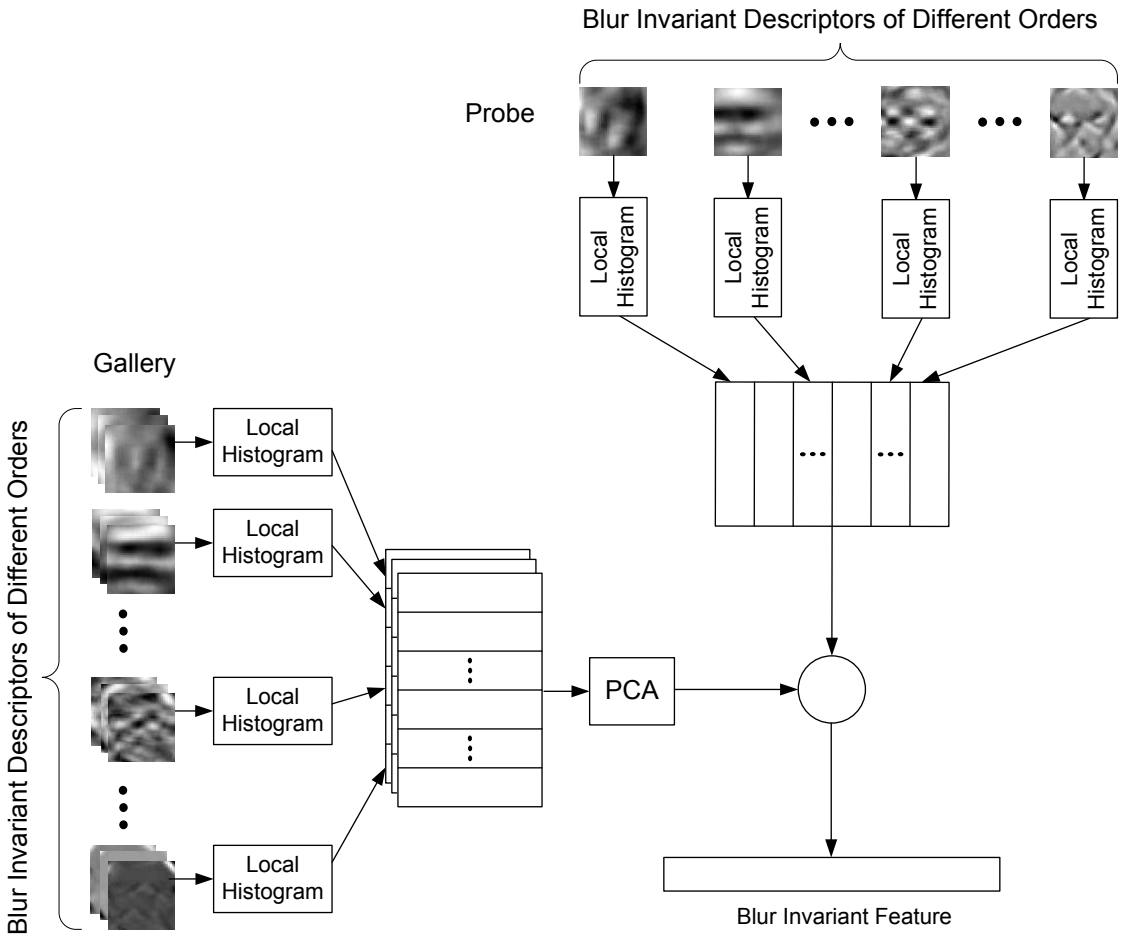


Figure 3.9: The Scheme for Local Histogram Approach

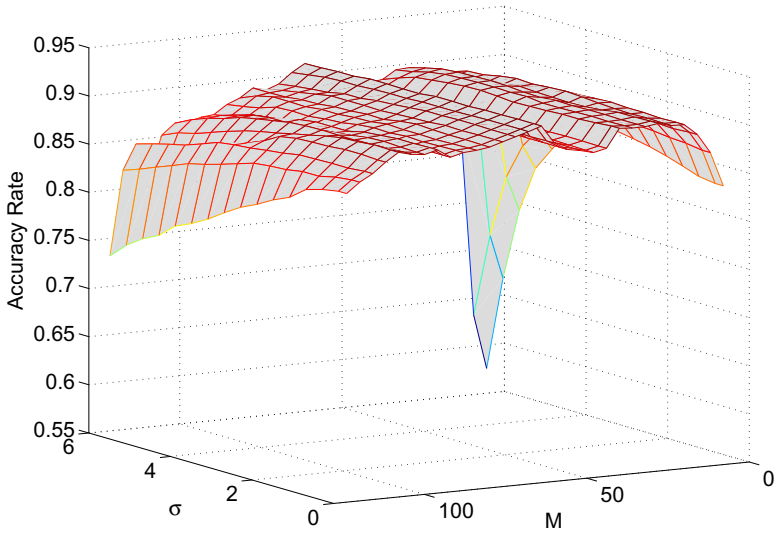


Figure 3.10: Accuracy rate of the EM scheme for the AT&T database. It shows the accuracy rate for different standard deviations and window sizes.

## 3.6 Experiment 2: Face Recognition with BIDs on AT&T Database

In this experiment, the AT&T database was employed. Similar to what was earlier explained in section 3.3, 5 out of 10 images per person were randomly chosen as the gallery set, and the rest were artificially blurred with Gaussian filters with different standard deviations to model different intensities of defocus blur. The standard deviation of the filters were changed from 0.2 to 5.8. BIDs of orders up to 11 (a total of 24 BIDs) were calculated. Also, the classifier was $k$-nn with $k = 1$ and MSSE as the measure.

In the first part of the experiment, the EM scheme was used as the feature extractor unit (Figure 3.1), $M$ was changed from 8 to 124, and the classification was done with 20 random allocations of gallery and probe sets. Figure 3.10 presents the average accuracy rates. The accuracy rate of the system stays fairly the same for the mid-range $M$s. Also, this value tends to remain the same with the increase of blur intensity. However, this behaviour changes as $M$ increases. The classification rate on sharp images begins to drop, and the sensitivity to blur intensity increases as well. The reason is that as the window size increases, the descriptors become more holistic,

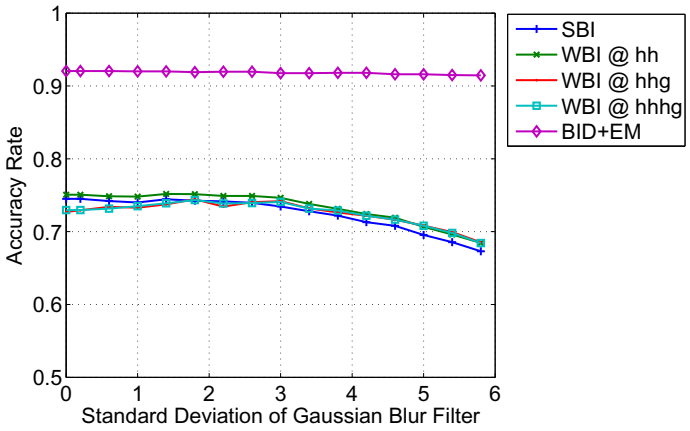


Figure 3.11: Accuracy rate comparison on the AT&T database versus blur intensity

losing concentration on local information. That is the problem with the blur invariants from the previous chapter as well, which were shown to have an unsatisfactory performance in section 3.3. When $M = 8$ and 12, the performance for high intensity blur is not good, the reason of which is the involvement of neighbouring pixels due to a large blur operator, that do not fall into the same window.

Figure 3.11 shows the best accuracy rates with the EM scheme, which was obtained when $M = 64$. The accuracy rates obtained with wavelet domain and spatial domain based invariants are also depicted in this figure. It is clear that the proposed scheme outperforms the other methods; the classification rate for sharp images is at 0.9205 and it drops to 0.9145 where $\sigma$ is equal to 5.8, a total of 0.6% drop in the accuracy rate.

In the second part, the local histogram scheme was employed for the same experiment, while $M$ was changed from 8 to 64. The number of bins were set to 7, and rectangular regions to be 8×8. The number of regions depends on $M$. In this experiment, it changed from 228 regions for $M = 8$ to 66 for $M = 64$. Figure 3.10 shows the average accuracy rates of the system for different $M$s and $\sigma$s. Except the cases for $M = 8$ and 12, the system presents a very robust performance versus the blur intensity changes.

Figure 3.13 shows the best classification rate with the local histogram scheme, which is yielded when $M = 32$. Other results are also shown for the sake of comparison. It is clear that the local histogram scheme is performing even better than the EM scheme. The classification rate for sharp images is 0.9365, and when $\sigma$ is 5.8, the accuracy drops to 0.9275.

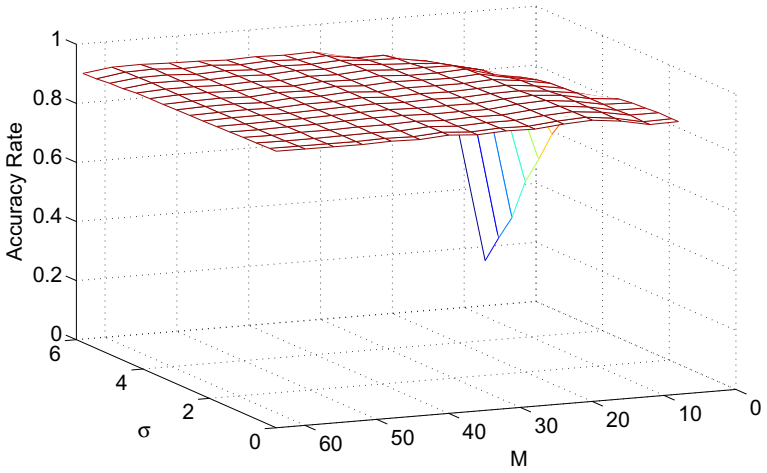


Figure 3.12: Accuracy rate of the local histogram scheme for the AT&T database. It shows the accuracy rate for different standard deviations and window sizes.

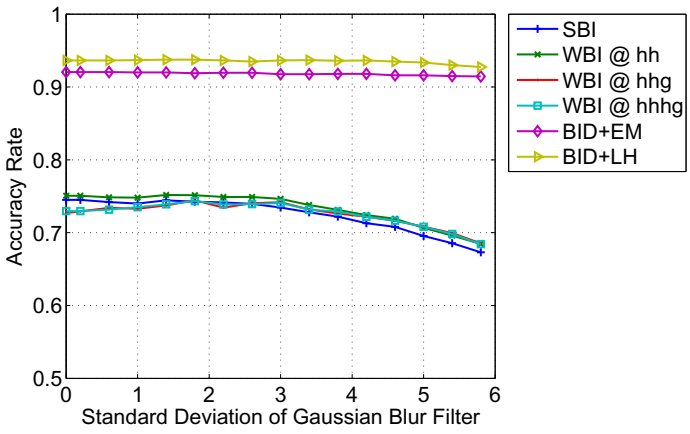


Figure 3.13: Accuracy rate comparison on the AT&T database versus blur intensity. LH stands for local histogram.


Figure 3.14: Samples from the FRGC 1.0.4 experiment

## 3.7 Experiment 3: Face Recognition with BIDs on FRGC Database

This experiment was carried out on the Face Recognition Grand Challenge (FRGC) [62]. There are standard experiments defined on this database in order to address different challenges. The sets of images that are allocated to each experiment are divided into three subsets with no overlaps: train, gallery, and probe. Such an allocation makes a fair comparison possible. The FRGC 1.0.4 experiment is selected for this part, since it has images in the probe set that are captured in controlled and uncontrolled conditions, making many of them blurry or with severe illumination changes. This is while all of the images in the gallery set are taken under controlled situations. The other point that makes this problem more challenging is the fact that there is only one sample per subject in the gallery set, with a total of 152 subjects. The probe set includes 608 images of these subjects.
The images of one of the subjects are shown in Figure 3.14. The first image is from the gallery set, and the rest are in the probe set. The database also provides the ground truth of the images. In this experiment, the coordination of the centres of eyes and mouths were used in order to crop the images. The process was as follows:

1. calculate the angle ($\alpha$) between the $x$-axis and a line that passes through both eyes,
2. tilt the image $\alpha$ degrees to straighten the face,


Figure 3.15: Samples from the FRGC 1.0.4 experiment after cropping

3. find the distance between the two eyes, and call it $d_1$,

4. call the point that is at the exact distance from both eyes $p$, find the distance between $p$ and the mouth, and call it $d_2$,

5. put $d$ equal to $2\max(d_1, d_2)$,

6. find the point that is at the exact distance from point $p$ and the mouth, and call it $o$.

7. crop a square of size $d \times d$ with its centre at $o$.

Figure 3.15 shows the images in Figure 3.14 after cropping. All of the images were resized to 128×128 after cropping, and their BIDs were calculated up to order 9 (a total of 18 BIDs). The BIDs were employed in the two proposed schemes to produce the required feature vectors for classification. Similar to the other experiments in this chapter, $k$-nn was used as the classifier with $k = 1$.
The results are reported in Table 3.1. The best results were obtained with $M = 8$. Also the number of bins was equal to 2 and the regions were 6×6 in the local histogram scheme.
For the sake of comparison, the classification rate with the LPQ face descriptors [1], which have received a broad interest in the literature, are also presented in this table. The classifier that was used in that work was also $k$-nn with $k = 1$. The reported classification rate with the LPQ face descriptors on this experiment is 45.90%. Using a preprocessing technique for decreasing the illumination effect, the classification rate was boosted up to 74.5%. This rate was later increased by

Table 3.1: Classification Rate on the FRGC 1.0.4 Experiment

| Method | Accuracy Rate(%) | Ref. |
|---|---|---|
| LPQ | 45.90 | [1] |
| LPQ w/ PP | 74.50 | [1] |
| Deblur + LPQ w/ PP | 79.60 | [25] |
| BID + EM | 70.23 | – |
| BID + LH | 79.77 | – |
| BID + EM(w/ One BID) | 64.97 | – |
| BID + LH(w/ One BID) | 65.95 | – |

5.1% using a deblurring technique [25] prior to calculation of LPQs.

This is while the recognition rate with the EM scheme is at 70.23%, which is significantly better than what LPQ could offer on its own. With the local histogram scheme, the recognition rate is at 79.77%, which is even higher than when LPQ was applied on enhanced and deblurred images. It should be reiterated that no preprocessing method was used in the proposed techniques. The table also reports the best classification rates that were achieved with only one BID. As it reads, the classification rates are again considerably better than what could be achieved with LPQ. It should be mentioned that the cropping process in [1] and [25] are different than what is used here. However, it is not expected to see a significant variation in classification rate with a change in the face cropping process.

In contrary to the conclusion in the Experiment 1, the best results were acquired when $M = 8$ in both schemes. As it was explained earlier, the smaller $M$ is, the more localized BIDs become. It means that more information is extractable with smaller window sizes. Also, the present blur in the images of the FRGC 1.0.4 experiment is not as severe as it was artificially produced in the previous experiment, meaning that the blur intensity is still in a range that is tolerable by $BID_{p,q}^{8\times8}$. Using a blur intensity inferring method, M. Nishyama et.al [53] reported that the median of blur intensity of the blurred images in this experiment is 2.5 ($\sigma = 2.5$). Considering these two points, a better accuracy rate with $M = 8$ in the FRGC 1.0.4 experiment sounds reasonable.

## 3.8 Conclusion

In this chapter, it has been shown that the spatial domain and the wavelet domain blur invariant moments are not powerful enough to be used in face recognition problems. This is mostly due to the non-orthogonal bases for moments. However, it was shown that with an alternative definition for moments, it is possible to increase the discriminative power to a great extent. Using the generalized ordinary moment definition, the blur invariants were redefined, and with the use of the two proposed schemes superb results have been achieved.

The proposed schemes were evaluated in two experiments. In the first one, the AT&T database was artificially blurred with different blur filters in order to study the blur effect on the accuracy rates of the proposed schemes. The analyses proved a very high classification rate along with a high robustness to blur variation. The classification rate with the EM scheme was at 92.05% and a considerable change in the blur intensity only could reduce this rate by 0.6%. Similarly, the local histogram scheme performed very well with a very little drop in the classification rate: 93.65% to 92.75% for a change of standard deviation of the Gaussian filter from 0 (no blur) to 5.8.

The second experiment was carried out on the FRGC database. The images in the probe set were taken under uncontrolled conditions, which made them blurry or poorly lightened. The classification result with the blur invariant LPQ technique was way less than what the proposed approaches achieved. A 33% improvement in classification rate using the proposed techniques proves their superiority. Even the use of a preprocessing algorithm for enhancing the images could only boost the LPQ face descriptors to show a better performance than the EM scheme. This is while the local histogram scheme still preformed better than LPQ with preprocessing. Finally, employing a deblurring technique made it possible to stand close to the proposed method, which was still marginally better. Not using any technique for reducing the illumination and/or blur effects shows that not only the proposed BIDs are invariant to blur, but also they allow changes in the lightening condition, which is not usually under control in a face recognition system, making them an excellent candidate for real-world face recognition problems.

# Chapter 4

# *Conclusions and Future Work*

The final chapter is devoted to discussion and conclusion on the dissertation. Also, the unanswered questions and possible directions for further research on the topic are introduced as the future work.

## 4.1 Conclusions

This dissertation is based on answering two questions that were asked in the first chapter: 1) is it possible to develop moment based blur invariants in the wavelet domain, and 2) how useful are the moment based blur invariants in face recognition?

The first question was answered in chapter 2. The models of most of the present blurs in images, such as defocus and motion effects, are centrally symmetric. The development of all of the moment based blur invariants depends on this assumption. As the first step, the blur invariant in the wavelet domain were developed for 1D continuous signals. Shift invariance is one of the basic properties that different types of invariants are expected to have. However vanishing moments of wavelet functions make it impossible to use the conventional definition of centroid since the denominator becomes zero. The problem was solved by proposing a generalized definition for centroid that can be used for all types of signals.

After showing the plausibility of the wavelet domain blur invariants, they were developed for 1D discrete signals. The problem with developing these invariants in the wavelet domain was to keep the shift invariant property, which was at risk this time by the employed transform; the discrete

wavelet transform does not preserve this property. This problem was overcome by replacing DWT with á trous algorithm. The development of wavelet domain blur invariants for 2D discrete signals was only a matter of expanding those for 1D discrete signals.

The performance of the proposed invariants was evaluated in different experiments. Their response to blur variation was tested in several examples, which showed that they are truly blur invariant. The blur invariants were used in a registration problem with real-world blurred images. The reported results showed that the proposed features are very robust to blur effects and intensity changes. The effect of noise was studied as well. In the related experiments, wavelet domain blur invariants performed better than their spatial domain counterparts. The choice of wavelet decomposition branch was the reason behind this variation. Minding this effect, it is possible to always have superior blur invariants in the wavelet domain than in the spatial domain.

One of the interesting points about the wavelet domain blur invariants is that they engulf those in the spatial domain as a special case. This was mathematically proved. Also, it was explained that how the proposed invariants do not have the null space that their counterpart could suffer from. The proposed materials in chapter 2 were published in [42, 44, 43].

The second question was answered in chapter 3. In that chapter, the wavelet and spatial domain blur invariants were employed for face recognition with blurred images. The preliminary results were not promising by any means. The superiority of the wavelet domain based blur invariants in chapter 2 changed to a marginally better performance in comparison to spatial domain blur invariants. The reason behind an unsatisfactory performance was found to be the poor bases that the geometric moments are developed on. Since the main limitation of the ordinary moments is because of their globality, with proposing a generalized definition for geometric moment, a more localized concentration was made possible. Blur invariants were redefined using this new definition, and it was analytically shown that how the descriptors respond to blur.

Two different schemes were proposed in order to take advantage of the blur invariant descriptors. Based on the experiments, it can be concluded that the window size in calculating the generalized ordinary moments affects the recognition rate. As the window size increases, the generalized ordinary moments tend to become like the conventional ordinary moments. Also, a very small window size make the blur invariant descriptors more susceptible to blur intensity.

A comparison with the state of the art (the LPQ face descriptors in this work) shows that the proposed technique is performing much better. The proposed method's recognition rate on the FRGC 1.0.4 experiment was 79.60%, compared to the reported recognition rate using the LPQ face descriptors with no preprocessing at 45.90%. What made it superior was the fact that the proposed

technique performed even better than when the LPQ face descriptors were used on enhanced images.

## 4.2 Future Work

This dissertation has two main contributions: wavelet domain blur invariants and blur invariant descriptors based on generalized ordinary moments. Although the superiority of the proposed techniques are demonstrated through experiments and discussions, it is still possible to improve them by further research.

The proposed wavelet domain blur invariants are based on geometric moments. There is a possibility of using complex moments in order to have phase information as well. It is then possible to develop blur invariants similar to those in the Fourier domain.

The wavelet functions that were used in the experiments of this dissertation were all compact. It is worth studying the effect of other types of wavelet functions. A comprehensive study on the effect of such changes in different application is interesting. Also, it might be possible to analytically learn the effect of different types of wavelet functions.

It was demonstrated in this dissertation that the branches that represent the high frequency information of image are not useful in the presence of noise. However, they still carry some properties that could be helpful in some application, which requires more investigation.

The blur invariant descriptors are calculated with the generalized ordinary moments. It would cut the computation to some extent if they were calculated directly from images.

The blur invariant descriptors were used in two different schemes in order to make the small enough to be suitable for classifiers. The two techniques that were employed were PCA and local histogram. There are, however, many other alternatives available that could prove more suitable.

It is always possible to substitute the geometric moments with orthogonal ones. Considering the latest finding by Kautsky and Flusser [30], developing the blur invariant descriptors that are proposed in this dissertation could be simpler. It is recommended to investigate the effect of such substitutions in a similar application.

The proposed blur invariant descriptors for faces are developed in the spatial domain. Considering the findings of chapter 2, It would be very simple to develop them in the wavelet domain as well to take advantage of the properties of that domain.

# References


[1] T. Ahonen, E. Rahtu, V. Ojansivu, and J. Heikkilä. Recognition of blurred faces using local phase quantization. In *Pattern Recognition, 2008. ICPR 2008. 19th International Conference on*, pages 1–4. IEEE, 2008.

[2] R. G. Andrzejak, K. Lehnertz, F. Mormann, Ch. Rieke, P. David, and Ch. E. Elger. Indications of nonlinear deterministic and finite-dimensional structures in time series of brain electrical activity: Dependence on recording region and brain state. *Phys. Rev. E*, 64(6):061907, Nov 2001.

[3] Y. Bentoutou and N. Taleb. Automatic extraction of control points for digital subtraction angiography image enhancement. *Nuclear Science, IEEE Transactions on*, 52(1):238 – 246, February 2005.

[4] Y. Bentoutou, N. Taleb, K. Kpalma, and J. Ronsin. An automatic image registration for applications in remote sensing. *Geoscience and Remote Sensing, IEEE Transactions on*, 43(9):2127 – 2137, September 2005.

[5] Y. Bentoutou, N. Taleb, M. Chikr El Mezouar, M. Taleb, and L. Jetto. An invariant approach for image registration in digital subtraction angiography. *Pattern Recognition*, 35(12):2853 – 2865, 2002.

[6] A. P. Bradley. Shift invariance in the discrete wavelet transform. In *In VIIth Digit. Image Comp*, pages 29–38, 2003.

[7] F. M. Candocia. Moment relations and blur invariant conditions for finite-extent signals in one, two and n-dimensions. *Pattern Recognition Letters*, 25(4):437–447, 2004.

[8] T.F. Chan and C.K. Wong. Total variation blind deconvolution. *Image Processing, IEEE Transactions on*, 7(3):370–375, 1998.

[9] R. Chellappa, P. Sinha, and P.J. Phillips. Face recognition by computers and humans. *Computer*, 43(2):46 –55, feb. 2010.

[10] X. Dai, H. Zhang, H. Shu, and L. Luo. Image recognition by combined invariants of legendre moment. In *Information and Automation (ICIA), 2010 IEEE International Conference on*, pages 1793 –1798, June 2010.

[11] I. Daubechies. *Ten lectures on wavelets*. Society for Industrial and Applied Mathematics, Philadelphia, PA, USA, 1992.

[12] I. Daubechies. Wavelet transforms and orthonormal wavelet bases. In *Proceedings of symposia in applied mathematics*, volume 47, 1993.

[13] C. Fiche, P. Ladret, and N.-S. Vu. Blurred face recognition algorithm guided by a no-reference blur metric. *Proceedings of SPIE - The International Society for Optical Engineering*, 7538, 2010.

[14] J. Flusser, J. Boldys, and B. Zitova. Moment forms invariant to rotation and blur in arbitrary number of dimensions. *Pattern Analysis and Machine Intelligence, IEEE Transactions on*, 25(2):234 – 246, Feb 2003.

[15] J. Flusser, J. Kautsky, and F. Šroubek. Implicit moment invariants. *International journal of computer vision*, 86(1):72–86, 2010.

[16] J. Flusser and T. Suk. Classification of degraded signals by the method of invariants. *Signal Processing*, 60(2):243 – 249, 1997.

[17] J. Flusser and T. Suk. Degraded image analysis: an invariant approach. *Pattern Analysis and Machine Intelligence, IEEE Transactions on*, 20(6):590 –603, Jun 1998.

[18] J. Flusser, T. Suk, and S. Saic. Image features invariant with respect to blur. *Pattern Recognition*, 28(11):1723 – 1732, 1995.

[19] J. Flusser, T. Suk, and S. Saic. Recognition of blurred images by the method of moments. *Image Processing, IEEE Transactions on*, 5(3):533 – 538, Mar 1996.

[20] J. Flusser, T. Suk, and B. Zitov. *Moments and moment invariants in pattern recognition*. Wiley Online Library, 2009.

[21] J. Flusser and B. Zitová. Combined invariants to linear filtering and rotation. *International Journal of Pattern Recognition and Artificial Intelligence*, 13(8):1123–1136, 1999.

[22] A.S. Georghiades, P.N. Belhumeur, and D.J. Kriegman. From few to many: Illumination cone models for face recognition under variable lighting and pose. *IEEE Trans. Pattern Anal. Mach. Intelligence*, 23(6):643–660, 2001.

[23] B.K. Gunturk, A.U. Batur, Y. Altunbasak, III Hayes, M.H., and R.M. Mersereau. Eigenface-domain super-resolution for face recognition. *Image Processing, IEEE Transactions on*, 12(5):597 – 606, May 2003.

[24] J. Haddadnia, M. Ahmadi, and K. Faez. An efficient feature extraction method with pseudo-zernike moment in rbf neural network-based human face recognition system. *EURASIP journal on applied signal processing*, 2003:890–901, 2003.

[25] A. Hadid, M. Nishiyama, and Y. Sato. Recognition of blurred faces via facial deblurring combined with blur-tolerant descriptors. In *Pattern Recognition (ICPR), 2010 20th International Conference on*, pages 1160–1163. IEEE, 2010.

[26] M-K. Hu. Visual pattern recognition by moment invariants. *Information Theory, IRE Transactions on*, 8(2):179 –187, February 1962.

[27] G. Hua, M-H. Yang, E. Learned-Miller, Y. Ma, M. Turk, D. J. Kriegman, and Th. S. Huang. Introduction to the special section on real-world face recognition. *IEEE Transactions on Pattern Analysis and Machine Intelligence*, 33:1921–1924, 2011.

[28] H. Ji and H. Zhu. Degraded image analysis using zernike moment invariants. *Acoustics, Speech and Signal Processing, 2009. ICASSP 2009. IEEE International Conference on*, pages 1941 –1944, april 2009.

[29] W. D. Jones. Computerized face-recognition technology is still easily foiled by cosmetic surgery. *IEEE Spectrum magazine*, 2009.

[30] J. Kautsky and J. Flusser. Blur invariants constructed from arbitrary moments. *Image Processing, IEEE Transactions on*, (99):1–1, 2011.

[31] N. Kingsbury. Complex wavelets and shift invariance. *Time-scale and Time-Frequency Analysis and Applications (Ref. No. 2000/019), IEE Seminar on*, pages 5/1 –510, 2000.

[32] D. Kundur and D. Hatzinakos. Blind image deconvolution. *Signal Processing Magazine, IEEE*, 13(3):43 –64, may 1996.

[33] G. Lafruit, F. Catthoor, J.P.H. Cornelis, and H.J. De Man. An efficient vlsi architecture for 2-d wavelet image coding with novel image scan. *Very Large Scale Integration (VLSI) Systems, IEEE Transactions on*, 7(1):56–68, 1999.

[34] M. Lang, H. Guo, J.E. Odegard, C.S. Burrus, and Jr. Wells, R.O. Noise reduction using an undecimated discrete wavelet transform. *Signal Processing Letters, IEEE*, 3(1):10 –12, Jan 1996.

[35] K. N. Le, K. P. D., and G. K. Egan. Hyperbolic wavelet power spectra of nonstationary signals. *Optical Engineering*, 42(10):3017–3037, 2003.

[36] K. N. Le, K. P. D., and G. K. Egan. Hyperbolic wavelet family. *Review of Scientific Instruments*, 75(11):4678–4693, 2004.

[37] K. N. Le, K. P. Dabke, and G. K. Egan. On mathematical derivations of auto-term functions and signal-to-noise ratios of the choi-williams, first- and nth-order hyperbolic kernels. *Digital Signal Processing*, 16(1):84 – 104, 2006.

[38] S.Z. Li and A.K. Jain. *Handbook of face recognition*. Springer, 2011.

[39] J. Liu and T. Zhang. Recognition of the blurred image by complex moment invariants. *Pattern Recognition Letters*, 26(8):1128 – 1138, 2005.

[40] A. Sethuram M. Albert and K. Ricanek. Implications of adult facial aging on biometrics. *Biometrics - Unique and Diverse Applications in Nature, Science, and Technology,*, pages 89–106, 2011.

[41] B. Mahdian and S. Saic. Detection of copy-move forgery using a method based on blur moment invariants. *Forensic Science International*, 171(2-3):180 – 189, 2007.

[42] I. Makaremi and M. Ahmadi. Blur invariants: A novel representation in the wavelet domain. *Pattern Recognition*, 43(12):3950 – 3957, 2010.

[43] I. Makaremi and M. Ahmadi. Wavelet domain blur invariants for image analysis. *Image Processing, IEEE Transactions on*, (99):1–1, 2011.

[44] I. Makaremi, K. Leboeuf, and M. Ahmadi. Wavelet domain blur invariants for 1d discrete signals. In Mohamed Kamel and Aurélio C. Campilho, editors, *ICIAR (1)*, volume 6753 of *Lecture Notes in Computer Science*, pages 69–79. Springer, 2011.

[45] S. Mallat. Zero-crossings of a wavelet transform. *Information Theory, IEEE Transactions on*, 37(4):1019 –1033, Jul 1991.

[46] S. Mallat. *A Wavelet Tour of Signal Processing, Second Edition (Wavelet Analysis & Its Applications)*. Academic Press, 2 edition, September 1999.

[47] S. Mallat and S. Zhong. Characterization of signals from multiscale edges. *Pattern Analysis and Machine Intelligence, IEEE Transactions on*, 14(7):710 –732, Jul 1992.

[48] S.G. Mallat. A theory for multiresolution signal decomposition: The wavelet representation. *Pattern Analysis and Machine Intelligence, IEEE Transactions on*, 11(7):674–693, 1989.

[49] P. McCanny, Sh. Masud, and J. McCanny. Design and implementation of the symmetrically extended 2-d wavelet transform. In *Acoustics, Speech, and Signal Processing (ICASSP), 2002 IEEE International Conference on*, volume 3, pages III–3108 –III–3111, may 2002.

[50] S. Metari and F. Deschenes. New classes of radiometric and combined radiometric-geometric invariant descriptors. *Image Processing, IEEE Transactions on*, 17(6):991 –1006, june 2008.

[51] A. Nabatchian, E. Abdel-Raheem, and M. Ahmadi. Human face recognition using different moment invariants: A comparative study. In *Image and Signal Processing, 2008. CISP'08. Congress on*, volume 3, pages 661–666. IEEE, 2008.

[52] S.A. Nene, S.K. Nayar, and H. Murase. Columbia object image library (coil-100). *Techn. Rep. No. CUCS-006-96, dept. Comp. Science, Columbia University*, 1996.

[53] M. Nishiyama, A. Hadid, H. Takeshima, J. Shotton, T. Kozakaya, and O. Yamaguchi. Facial deblur inference using subspace analysis for recognition of blurred faces. *IEEE transactions on pattern analysis and machine intelligence*, pages 838–845, 2011.

[54] M. Nishiyama, H. Takeshima, J. Shotton, T. Kozakaya, and O. Yamaguchi. Facial deblur inference to improve recognition of blurred faces. In *Computer Vision and Pattern Recognition, 2009. CVPR 2009. IEEE Conference on*, pages 1115–1122. IEEE, 2009.

[55] V. Ojansivu and J. Heikkilä. Image registration using blur-invariant phase correlation. *Signal Processing Letters, IEEE*, 14(7):449 –452, July 2007.

[56] V. Ojansivu and J. Heikkilä. A method for blur and similarity transform invariant object recognition. In R. Cucchiara, editor, *ICIAP*, pages 583–588. IEEE Computer Society, 2007.

[57] V. Ojansivu and J. Heikkilä. Object recognition using frequency domain blur invariant features. In Bjarne K. Ersbøll and Kim Steenstrup Pedersen, editors, *SCIA*, volume 4522 of *Lecture Notes in Computer Science*, pages 243–252. Springer, 2007.

[58] Ville Ojansivu and Janne Heikkilä. Blur insensitive texture classification using local phase quantization. In Abderrahim Elmoataz, Olivier Lezoray, Fathallah Nouboud, and Driss Mammass, editors, *ICISP*, volume 5099 of *Lecture Notes in Computer Science*, pages 236–243. Springer, 2008.

[59] A. Papoulis. *Probability, Random Variables, and Stochastic Processes*. New York : McGraw-Hill Book Company, 1965.

[60] K.K. Parhi and T. Nishitani. Vlsi architectures for discrete wavelet transforms. *Very Large Scale Integration (VLSI) Systems, IEEE Transactions on*, 1(2):191–202, 1993.

[61] M. Pedone and J. Heikkilä. Blur and contrast invariant fast stereo matching. In J. Blanc-Talon, S. Bourennane, W. Philips, D. C. Popescu, and P. Scheunders, editors, *ACIVS*, volume 5259 of *Lecture Notes in Computer Science*, pages 883–890. Springer, 2008.

[62] P.J. Phillips, P.J. Flynn, T. Scruggs, K.W. Bowyer, J. Chang, K. Hoffman, J. Marques, J. Min, and W. Worek. Overview of the face recognition grand challenge. In *Computer vision and pattern recognition, 2005. CVPR 2005. IEEE computer society conference on*, volume 1, pages 947–954. IEEE, 2005.

[63] G. Ramponi. A cubic unsharp masking technique for contrast enhancement. *Signal Processing*, 67(2):211–222, 1998.

[64] Th. H. Reiss. *Recognizing Planar Objects Using Invariant Image Features*. Springer-Verlag New York, Inc., Secaucus, NJ, USA, 1993.

[65] M. Ibrahim Sezan and A. Murat Tekalp. Survey of recent developments in digital image restoration. *Optical Engineering*, 29(5):393–404, 1990.

[66] A. Shahbahrami, B. Juurlink, and S. Vassiliadis. Implementing the 2-d wavelet transform on simd-enhanced general-purpose processors. *Multimedia, IEEE Transactions on*, 10(1):43–51, 2008.

[67] M. J. Shensa. The discrete wavelet transform: wedding the a trous and mallat algorithms. *IEEE Transactions on Signal Processing*, 40(10):2464–2482, Oct 1992.

[68] I. Stainvas and N. Intrator. Blurred face recognition via a hybrid network architecture. *Pattern Recognition, 2000. Proceedings. 15th International Conference on*, 2:805 –808 vol.2, 2000.

[69] T. Suk and J. Flusser. Features invariant simultaneously to convolution and affine transformation. In Wladyslaw Skarbek, editor, *CAIP*, volume 2124 of *Lecture Notes in Computer Science*, pages 183–190. Springer, 2001.

[70] D.S. Taubman, M.W. Marcellin, and M. Rabbani. Jpeg2000: Image compression fundamentals, standards and practice. *Journal of Electronic Imaging*, 11:286, 2002.

[71] C.H. Teh and R.T. Chin. On image analysis by the methods of moments. *Pattern Analysis and Machine Intelligence, IEEE Transactions on*, 10(4):496–513, 1988.

[72] M. Turk and A. Pentland. Eigenfaces for recognition. *Journal of cognitive neuroscience*, 3(1):71–86, 1991.

[73] F.W. Wheeler, Xiaoming Liu, and P.H. Tu. Multi-frame super-resolution for face recognition. *Biometrics: Theory, Applications, and Systems, 2007. BTAS 2007. First IEEE International Conference on*, pages 1 –6, sep. 2007.

[74] J. Wood. Invariant pattern recognition: A review. *Pattern Recognition*, 29(1):1 – 17, 1996.

[75] F. Xin, Zh. Qi, L. Dequn, and Zh. Ling. Face image restoration based on statistical prior and image blur measure. In *Multimedia and Expo, 2003. ICME '03. Proceedings. 2003 International Conference on*, volume 3, pages III – 297–300 vol.3, july 2003.

[76] H. Zhang, H. Shu, G.N. Han, G. Coatrieux, L. Luo, and J.L. Coatrieux. Blurred image recognition by legendre moment invariants. *Image Processing, IEEE Transactions on*, 19(3):596 –611, march 2010.

# Appendix A

## *IEEE Permission for Reprint*

# Appendix B

## *Springer Permission for Reprint*

SPRINGER LICENSE
TERMS AND CONDITIONS

Jan 26, 2012

This is a License Agreement between Iman Makaremi ("You") and Springer ("Springer") provided by Copyright Clearance Center ("CCC"). The license consists of your order details, the terms and conditions provided by Springer, and the payment terms and conditions.

**All payments must be made in full to CCC. For payment instructions, please see information listed at the bottom of this form.**

| | |
|---|---|
| License Number | 2836560285111 |
| License date | Jan 26, 2012 |
| Licensed content publisher | Springer |
| Licensed content publication | Springer eBook |
| Licensed content title | Wavelet Domain Blur Invariants for 1D Discrete Signals |
| Licensed content author | Iman Makaremi |
| Licensed content date | Jun 30, 2011 |
| Type of Use | Thesis/Dissertation |
| Portion | Full text |

| | |
|---|---|
| Number of copies | 999 |
| Author of this Springer article | Yes and you are the sole author of the new work |
| Order reference number | |
| Title of your thesis / dissertation | Face Recognition with Degraded Images |
| Expected completion date | Jan 2012 |
| Estimated size(pages) | 83 |
| Total | 0.00 USD |

Terms and Conditions

**If you would like to pay for this license now, please remit this license along with your payment made payable to "COPYRIGHT CLEARANCE CENTER" otherwise you will be invoiced within 48 hours of the license date. Payment should be in the form of a check or money order referencing your account number and this invoice number RLNK500706909.**
**Once you receive your invoice for this order, you may pay your invoice by credit card. Please follow instructions provided at that time.**
**Make Payment To:**

**Copyright Clearance Center**
**Dept 001**
**P.O. Box 843006**
**Boston, MA 02284-3006**

**For suggestions or comments regarding this order, contact RightsLink Customer Support: customercare@copyright.com or +1-877-622-5543 (toll free in the US) or +1-978-646-2777.**
**Gratis licenses (referencing $0 in the Total field) are free. Please retain this printable license for your reference. No payment is required.**

**SPRINGER LICENSE**
**TERMS AND CONDITIONS**

Jan 26, 2012

This is a License Agreement between Iman Makaremi ("You") and Springer ("Springer") provided by Copyright Clearance Center ("CCC"). The license consists of your order details, the terms and conditions provided by Springer, and the payment terms and conditions.

**All payments must be made in full to CCC. For payment instructions, please see information listed at the bottom of this form.**

| | |
|---|---|
| License Number | 2836560285111 |
| License date | Jan 26, 2012 |
| Licensed content publisher | Springer |
| Licensed content publication | Springer eBook |
| Licensed content title | Wavelet Domain Blur Invariants for 1D Discrete Signals |
| Licensed content author | Iman Makaremi |
| Licensed content date | Jun 30, 2011 |
| Type of Use | Thesis/Dissertation |
| Portion | Full text |
| Number of copies | 999 |
| Author of this Springer article | Yes and you are the sole author of the new work |
| Order reference number | |
| Title of your thesis / dissertation | Face Recognition with Degraded Images |
| Expected completion date | Jan 2012 |
| Estimated size(pages) | 83 |
| Total | 0.00 USD |
| Terms and Conditions | |

**If you would like to pay for this license now, please remit this license along with your payment made payable to "COPYRIGHT CLEARANCE CENTER" otherwise you will be invoiced within 48 hours of the license date. Payment should be in the form of a check or money order referencing your account number and this invoice number RLNK500706909.**
**Once you receive your invoice for this order, you may pay your invoice by credit card. Please follow instructions provided at that time.**

**Make Payment To:**
**Copyright Clearance Center**
**Dept 001**
**P.O. Box 843006**
**Boston, MA 02284-3006**

**For suggestions or comments regarding this order, contact RightsLink Customer Support: customercare@copyright.com or +1-877-622-5543 (toll free in the US) or +1-978-646-2777.**

**Gratis licenses (referencing $0 in the Total field) are free. Please retain this printable license for your reference. No payment is required.**

# *VITA AUCTORIS*

Iman Makaremi was born in 1981, in Babol, Iran. He received his B.Sc. degree in electrical engineering in 2004 from the University of Tehran, Tehran, Iran. He finished his masters in Electrical Engineering at the KN Toosi University of Technology, Tehran, Iran in 2007 in the area of Intelligent Fault Detection. Currently, he is working toward his Ph.D. in Electrical Engineering at the University of Windsor, Canada. His research interest includes geometric and radiometric invariant descriptors and their applications in image processing and pattern recognition. In the following, there is a list of publications resulting from his dissertation research.

1. I. Makaremi and M. Ahmadi. Blur invariants: A novel representation in the wavelet domain. Pattern Recognition, 43(12):3950 3957, 2010.

2. I. Makaremi and M. Ahmadi. Wavelet domain blur invariants for image analysis.Image Processing, IEEE Transactions on, (99):11, 2011.

3. I. Makaremi, Karl Leboeuf, and Majid Ahmadi. Wavelet domain blur invariants for 1d discrete signals. In Mohamed Kamel and Aurelio C. Campilho, editors, ICIAR (1), volume 6753 of Lecture Notes in Computer Science, pages 6979. Springer, 2011.

4. I. Makaremi and Majid Ahmadi. Face Recognition with Blurred Images using an Alternative Definition for Moment based Blur Invariant Descriptors. *Submitted to* Pattern Recognition, 2011.